Impact of the Fine Minerals Particles on Pentlandite Flotation

by

Andreas Mako Kusuma

A thesis submitted in partial fulfillment of the requirements for the degree of

Master of Science

in
Materials Engineering

Department of Chemical and Materials Engineering
University of Alberta

Abstract

In this study, the interactions between pentlandite and gangue minerals (i.e. serpentine, olivine, magnesite) were investigated by directly measuring the zeta potential distributions. In addition, an atomic force microscope (AFM) was used to measure the interaction forces between a silicon nitride tip and gangue mineral surfaces. Flotation tests were performed to understand the impact of the fine gangue minerals on pentlandite recovery. The zeta potential distribution measurements indicated an attractive interaction between pentlandite and serpentine, and a repulsive interaction between pentlandite with both olivine and magnesite at about pH 10 in 10 mM KCl solution. AFM force measurements showed a repulsive interaction between an AFM tip with both serpentine and olivine surface, and a slight attraction between an AFM tip and a magnesite surface at pH 10 in 1 mM KCl solution. The repulsion between the tip and the serpentine surface is possibly due to the measurement being performed on the silica face of serpentine. The presence of olivine and magnesite did not show detrimental effect on pentlandite recovery, as opposed to the pentlandite depression observed in the presence of serpentine during the flotation at pH 10 in 5×10^{-4} M PAX solution. Similarly, the presence of serpentine also depresses pentlandite recovery at pH 2.5 in 5×10^{-4} M solution.

Preface

Chapter 3 of this thesis was submitted for publication to the *Minerals Engineering* journal as Kusuma, A.M., Zeng, H., and Liu, Q., "Understanding interaction mechanisms between pentlandite and gangue minerals by zeta potential and surface force measurements". I was responsible for the data collection and analysis as well as the manuscript composition. Zeng, H. contributed to manuscript edits. Liu, Q. was the supervisory author and was involved with concept formation.

Chapter 4 of this thesis will be sent for publication to the *Minerals Engineering* journal as Kusuma, A.M., Zeng, H., and Liu, Q., "Effect of the presence of fine minerals towards pentlandite flotation". I was responsible for the data collection and analysis as well as the manuscript composition. Zeng, H. contributed to manuscript edits. Liu, Q. was the supervisory author and was involved with concept formation.

Part of the Chapter 3 of this thesis was presented at the PROCEMIN 2013 International Mineral Processing Conference.

Acknowledgement

Finally, I dedicate this work to God, my father, my mother, my sister, my other family members, and to all of my friends. Without their support, I wouldn't have reached this far.

Table of Content

List of Tables

List of Figures

List of Symbols

A	Hamaker constant, J
c_o	Bulk ion number electrolyte concentration, m^{-3}
D	Separation distance between the substrate and the end of the AFM tip, m
e	Elementary charge ,C
F^{DLVO}	Total DLVO interaction force, N
F^{edl}	Electrostatic double layer force, N
F^{vdw}	Van der Waals forces, N
h	Planck's constant, J.s
k_B	Boltzmann constant, $J.K^{-1}$
L	Separation distance between the substrate and the differential surface section of the AFM tip, m
n_i	Refractive index of material i
r	Radius of the circle of the AFM tip at a given vertical position, m
R	Radius of the spherical cap at the end of the AFM tip, m
R_q	Root-mean-square roughness, nm
T	Temperature, K

v_v	Main absorption frequency in UV region, s^{-1}
α	Geometrical angle of the AFM tip (see Figure 3-1)
β	Geometrical angle of the AFM tip (see Figure 3-1)
ε	Permittivity of the solution
ε_i	Static dielectric constant for material i
ε_o	Permittivity of the vacuum, $F.m^{-1}$
κ^{-1}	Debye length, nm
ψ	Surface potential, mV
σ	Surface charge density, $C.m^{-2}$
θ	Contact angle, degree
ζ	Zeta potential, mV

List of Abbreviations

AES	Auger electron spectroscopy
AFM	Atomic force microscope
DLVO Theory	Theory developed by Derjaguin, Landau, Verwey, and Overbeek
EDX	Energy dispersive X-Ray spectroscopy
FE-SEM	Field emission-Scanning electron microscope
Mg	Magnesite (see Chapter 4)
Ol	Olivine (see Chapter 4)
PAX	Potassium amyl xanthate
Pn	Pentlandite (see Chapter 4)
sccm	Standard cubic centimetres per minute
SEM	Scanning electron microscope
Sp	Serpentine (see Chapter 4)
STM	Scanning tunneling microscope
TG	Thermogravimetry
WHO	World Health Organization

Chapter 1 Introduction

1.1 Uses and occurrence of nickel

Nickel is a silvery white metal, which was first isolated in 1751 by Baron Axel Fredrik Cronstedt (nickel (Ni), 2014). This metal is seldom used in its pure form; it is mostly used as an alloying components. The nickel alloys exhibit a high resistance to wear and corrosion (Minowa et al., 1989; Rahilly and Price, 2003; Zhang et al., 2005). The nickel alloys are also used in many high temperature environments, such as in the aircraft and power generation turbines (Pollock and Tin, 2006). Another common application of nickel is in electroplating. Nickel is deposited electrochemically on a substrate to form a corrosive resistant layer. Electroplating can be found in the coating of tank lining, inner wall of pipe, and in other chemical industry equipment (nickel (Ni), 2014).

Nickel deposits can be classified into two types: laterites and sulphides. There are several countries where the exploitation of the deposits is economically feasible, namely Russia, Canada, Australia, Indonesia, and New Caledonia (Alvarez-Silva, 2011). While nickel laterites account for about 70% of worldwide nickel resources, only about 40% of the world nickel production comes from laterites (Dalvi et al., 2004; Moskalyk and Alfantazi, 2002). This is mainly due to the high-cost and complex requirement for processing laterites (Mudd, 2010). In Canada, the major nickel deposits are located in Sudbury, Thompson, Voisey's Bay, and Raglan (Alvarez-Silva et al., 2010). A typical valuable nickel sulphide mineral is pentlandite [$(Ni,Fe)_9S_8$], and it is a source of much of world's nickel

supply (Edwards et al., 1980). Pentlandite is also associated with pyrrhotite ($Fe_{1-x}S$) and MgO-minerals as the dominant gangue minerals.

1.2 Challenges in the flotation of low-grade ultramafic nickel ore

As the high-grade nickel ores are declining, the low-grade ultramafic nickel ores, such as ores from Thompson deposit, are becoming important alternative sources for producing nickel (Dai et al., 2009; Merve Genc et al., 2012). These low-grade ultramafic nickel ores may also have significant economic value due to their significant quantity (Alvarez-Silva, 2011). However, the processing of such ores is proven to be challenging. This is due to the presence of the MgO-containing gangue minerals, mainly serpentine [$Mg_3Si_2O_5(OH)_4$].

The high pulp viscosity is a problem attributed to the presence of serpentine, which results in the flotation and grinding at low percent solids; hence increasing the processing cost (Dai et al., 2009). Serpentine is also responsible to the formation of air bubble-macro fibers aggregation, resulting in the recovery of MgO-containing minerals and lower nickel grade in concentrate (Xu et al., 2010). Another adverse impact due to the presence of serpentine is slime coating. Slime coating occurs when positively charged serpentine particles coat the surface of negatively charged pentlandite mainly by the electrostatic attractive interaction (Bremmel et al., 2005; Edwards et al., 1980). This results in the reduction of nickel grade in the concentrate as well as the loss of nickel recovery due to the slime coating on pentlandite (Alvarez-Silva, 2011).

The processing of low-grade ultramafic nickel ore generates more tailings per unit of valuable mineral recovered (Niederhauser and Wisdom, 2013). One polymorph of serpentine is the fibrous chrysotile. World Health Organization (WHO) classified chrysotile as carcinogenic to humans and put restriction on its use in structural materials (Nishikawa et al., 2008). Consequently, tailings from mining operations that contain chrysotile pose environmental hazard (Huang et al., 2013). Therefore the processing of low-grade ultramafic nickel ores requires a specific standard operating procedure for the worker's safety and to abide by environmental regulations.

In order to reduce or eliminate the problems associated with the low-grade ultramafic nickel ores, several processing procedures for such ores have been proposed. A processing of such ore using fiber disintegration by acid attack has been investigated (Uddin et al., 2012) to eliminate the problems caused by the serpentine fiber. The use of sodium hexametaphosphate has been reported to improve serpentine dispersion in the flotation of pyrite; hence improving the adsorption of xanthate on pyrite (Lu et al., 2011). Another flowsheet for processing Thompson ultramafic low-grade nickel ores has also been developed (Dai et al., 2009). An important component of this flowsheet is the utilization of hydrocyclones to deslime the ore after comminution. The cyclone overflow was discarded while the cyclone underflow was the flotation feed. Even though this method was an effective means of reducing the effect of slimes, the recovery of pyrrhotite was found to be increased, resulting in lower nickel grade of the concentrate. The increase in the pyrrhotite recovery was due to prolonged

oxidation during desliming and lack of slimes to coat and depress pyrrhotite during flotation (Dai et al., 2009). Minerals such as: molybdenite, realgar, and stibnite are easily floated without collectors or any special conditions for collectorless flotation; such minerals exhibit natural floatability (Hayes et al., 1987). For molybdenite, the edge plane is highly polar, whereas the basal plane is naturally hydrophobic (Hayes et al., 1987). A common sulphide mineral such as chalcopyrite, on the other hand, does not appear to exhibit natural floatability. However, a collectorless flotation of chalcopyrite can be performed in the presence of an applied open-circuit potential (Hayes and Ralston, 1988). Pentlandite's collectorless floatability appears to be relatively unstable and involves more factors such as the amount of associated pyrrhotite and the nature of its oxidation sensitivity (Kelebek et al., 1996). In typical nickel ore flotation, pyrrhotite is rejected to obtain high concentrates' grade and to minimize SO_2 emission during smelting. Some approaches to obtain pyrrhotite rejection include: raising flotation pH to partially depress pyrrhotite, introducing separate pyrrhotite rejection circuits, and using magnetic separation to remove pyrrhotite from flotation feed or concentrate (Bozkurt et al., 1999). Diethylenetriamine (DETA) has been identified as an effective pyrrhotite depressant (Bozkurt et al., 1999). In addition, a combined use of triethylenetetramine (TETA) and sodium metabisulfite (SMBS) showed an excellent separation between pentlandite and pyrrhotite, due to the low development of hydrophobic species on pyrrhotite surface and resulting in a better concentrates' grade (Kelebek and Tukel, 1999).

A more recent processing method utilizing a microwave pretreatment (Bobicki et al., 2014) has also been proposed. The microwave pretreatment can be seen as a mode of thermal pretreatment. The main purpose of this pretreatment is to convert the chemical structure of serpentine. Under thermal heating, serpentine is converted into olivine through dehydroxylation between 550-800 ^{o}C, as shown in the following reactions (Cattaneo et al, 2003):

$$Mg_3Si_2O_5(OH)_4 \rightarrow Mg_3Si_2O_7 + 2H_2O \qquad (1.1)$$

$$2Mg_3Si_2O_7 \rightarrow 3Mg_2SiO_4 + SiO_2 \qquad (1.2)$$
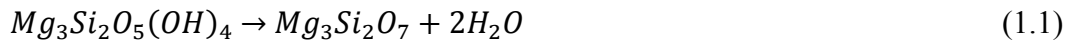
Microwave heating also shows higher efficiency as compared to conventional heating and it has benefits such as: rapid heating that starts from interior of a body (Haque, 1999). Previous studies have shown that microwave pretreatment improved the flotation of coal and ilmenite ores (Fan and Rowson, 2000; Wei et al., 2011). Microwave treatment affects coal surface properties by reacting the oxygen containing functional groups on the surface with the hydrogen or methane in the atmosphere during treatment, thereby changing its wettability (Wei et al., 2011). Microwave treatment also increases surface oxidation on ilmenite surface, leading to the enhancement of sodium oleate absorption (Fan and Rowson, 2000). The conversion of serpentine into olivine also helps to eliminate the presence of fibrous chrysotile, as observed by Huang et al. (2013). Therefore, microwave pretreatment can potentially reduce the environmental hazard as well as the health hazard to the workers who work with the low-grade ultramafic nickel ores.

In the flotation of low-grade ultramafic nickel ores, sodium carbonate is an optimal pH modifier to achieve the flotation pH of 10.1 (Dai et al., 2009). It should be noted that achieving this pH without the use of sodium carbonate may lead to the formation of magnesium hydroxide precipitates. These magnesium hydroxide precipitates are positively charged, which may form a combined serpentine/magnesium hydroxide slime coating on pentlandite surface (Alvarez-Silva, 2011; Sedore, 2003). Therefore, sodium carbonate is used to control the precipitation of magnesium hydroxide by sequestering magnesium to form magnesium carbonate or magnesite (Alvarez-Silva, 2011).

1.3 Intermolecular and surface forces

The interaction between different minerals during flotation is an essential factor that can affect the outcome of a flotation. Phenomenon in the flotation such as slime coating is the result of an electrostatic interaction between the gangue mineral and valuable mineral. Therefore, understanding the intermolecular and surface forces, such as van der Waals forces and electrostatic double layer force, is important to the interpretation of minerals interaction. The understanding of minerals interaction is an important and essential tool in the mineral flotation.

1.3.1 Van der Waals forces

The van der Waals forces, named after the Dutch physicist Johannes van der Waals (1837-1923), are the total effect of the attractive and repulsive forces between molecular entities excluding those due to bond formation or to the electrostatic interaction of ions or of ionic groups with one another or with neutral

molecules (Müller, 1994). The van der Waals forces include: dipole-dipole interaction (Keesom force), dipole-induced dipole interaction (Debye force), and instantaneous induced dipole-induced dipole interaction or dispersive interaction (London force) (Berg, 2010; Masliyah et al., 2011). The magnitude of van der Waals forces decays with increasing separation distance (D) between objects. The van der Waals forces acting between atoms and/or molecules are inversely proportional to D^{-6} (Butt et al., 2005). The van der Waals forces, however, are relatively weaker than the forces induced by covalent bonds or electrostatic interactions between ions. The van der Waals forces depend on the geometries of the two interacting objects. The expression for van der Waals forces between a sphere of radius (R) and a flat surface is given by $F = -AR/6D^2$ (Butt et al., 2005). The Hamaker constant A is defined as $A = \pi^2 C \rho_1 \rho_2$, where C is the constant in the atom-atom pair potential and ρ_1 and ρ_2 are the number of atoms per unit volume (Butt et al., 2005). The Hamaker constant depends on the nature of the interacting objects.

1.3.2 Electrostatic double layer force

The charging of a surface in a liquid includes several mechanisms: (1) preferential dissolution of surface ions, (2) direct ionization of surface groups, (3) isomorphic substitution of surface/lattice ions, (4) specific ion adsorption, and (5) charges deriving from anisotropic crystal lattice structures (Myers, 1999). The final surface charge of co-ions is balanced by equal and oppositely charged counter-ions. The layer formed by the bound counter-ions on the surface is called Stern or Helmholtz layer; whereas the diffuse atmosphere of counter-ions close to the

surface is known as the diffuse electric double layer (Israelachvili, 2011). The potential at the surface and that on the Stern layer are denoted as Ψ_o and Ψ_S, respectively. The diffuse electrical double layer obeys the Poisson-Boltzmann distribution:

$$d^2\Psi/dx^2 = -\sum_i(z_i e\rho_{i\infty}/\varepsilon_o\varepsilon)e^{-z_i e\Psi/kT} \qquad (1.3)$$

where x is the distance from Stern plane, z is the valence of ion, e is the elementary charge, ρ_∞ is the bulk counter-ions density, ε_o is the permittivity of vacuum, ε is the relative dielectric constant. For a practical point of view, the Debye-Hückel approximation is used:

$$\Psi = \Psi_S e^{-\kappa x} \qquad (1.4)$$

where the Debye length or the electrical double layer thickness is given by:

$$\frac{1}{\kappa} = \left(\frac{\varepsilon_o\varepsilon k_B T}{e^2\sum\rho_{i\infty}z_i{}^2}\right)^{1/2} \qquad (1.5)$$

The electrical double layers of two surfaces may overlap with each other when two surfaces with similar charge sign approaches towards each other. This overlapping generates repulsive force due to osmotic repulsion of the counter-ions in the electrical double layer. According to equation (1.5), by increasing the salt concentration, the electrical double layer will be reduced. In other word, the electrical double is compressed.

The surface potential cannot be measured experimentally (Masliyah et al., 2011). Therefore, zeta potential (ζ, V) becomes a very important characteristic of a charged surface. In the diffuse electrical double layer, a shear or slip plane exists

where the liquid starts moving relative to the surface. The potential measured at the shear plane is called zeta potential. The measurement of zeta potential is based on an electrokinetic phenomenon called electrophoresis. Suspended particles move when an electric field is applied. The electrophoretic mobility (μ_e, $m^2s^{-1}V^{-1}$) can be measured from the movement of these suspended particles. For a particle larger than 0.1 μm, the electrophoretic mobility is given by the Smoluchowski equation:

$$\mu_e = \frac{\varepsilon_o \varepsilon \zeta}{\eta} \qquad (1.6)$$

where η is the liquid dynamic viscosity (Pa.s), ε_o and ε is the permittivity of vacuum and medium, respectively ($CV^{-1}m^{-1}$). Since electrophoretic mobility can be measured from the instrument, equation (1.6) allows the conversion from electrophoretic mobility zeta potential.

1.4 Objectives

Considerable studies have been carried out, especially in examining the interaction between pentlandite and serpentine. However, there has been no study which considers other type of gangue minerals, such as olivine and magnesite. This thesis investigates the interaction between different gangue minerals and pentlandite, as the valuable nickel bearing mineral. This fundamental study was performed by using zeta potential distribution measurements and an atomic force microscope (AFM). The type of interaction between the gangue minerals and pentlandite can help to predict the outcome of the pentlandite flotation in the presence of these minerals. This study helps to better understand the problems and

issues in the mineral processing industry, especially in the nickel processing industry.

1.5 References

Alvarez-Silva, M. (2011) *Surface chemistry study on the pentlandite-serpentine system, PhD Dissertation*, McGill University.

Alvarez-Silva, M., Mirnezami, M., Uribe-Salas, A., Finch, J.A. (2010) 'Point of zero charge, isoelectric point and aggregation of phyllosilicate minerals', *Canadian Metallurgical Quarterly*, vol. 49, no. 4, pp. 405–410.

Berg, J.C. (2010) *An introduction to interfaces and colloids: The bridge to nanoscience*, World Scientific, Singapore.

Bobicki, E.R., Liu, Q., Xu, Z. (2014) 'Microwave heating of ultramafic nickel ores and mineralogical effects', *Minerals Engineering*, vol. 58, pp. 22-25.

Bozkurt, V., Xu, Z., Finch, J.A. (1999) 'Effect of depressants on xanthate adsorption on pentlandite and pyrrhotite: Single vs mixed minerals', *Canadian Metallurgical Quarterly*, vol. 38, no. 2, pp. 105-112.

Bremmel, K.E., Fornasiero, D., Ralston, J. (2005) 'Pentlandite-lizardite interactions and implications for their separation by flotation', *Colloids and Surfaces A: Physicochemical and Engineering Aspects*, vol. 252, pp. 207–212.

Butt, H.J., Cappella, B., Kappl, M. (2005) 'Force measurements with the atomic force microscope: Technique, interpretation and applications', *Surface Science Reports*, vol. 59, pp. 1–152.

Cattaneo, A., Gualtieri, A. F., Artioli, G. (2003) 'Kinetic study of the dehydroxylation of chrysotile asbestos with temperature by in situ XRPD', *Physics and Chemistry of Minerals*, vol. 30, no. 3, pp. 177-183.

Dai, Z., Bos, J.A., Quinn, P., Lee, A., Xu, M. (2009) 'Flowsheet development for Thompson ultramafic low-grade nickel ores', *Proceedings of the 48th annual conference of metallurgists of CIM*, Met Soc, Sudbury, Ontario, Canada, pp. 217–228.

Dalvi, A.D., Bacon, W.G., Osborne, R.C. (2004) 'The past and the future of nickel laterites', In *PDAC 2004 International Convention, Trade Show & Investors Exchange*, Toronto: The Prospectors and Developers Association of Canada, pp. 1–27.

Edwards, C.R., Kipkie, W.B., Agar, G.E. (1980) 'The effect of slime coatings of the serpentine minerals, chrysotile and lizardite, on pentlandite flotation', *International Journal of Mineral Processing*, vol. 7, pp. 33–42.

Fan, X., Rowson, N.A. (2000) 'Fundamental investigation of microwave pretreatment on the flotation of massive ilmenite ores', *Developments in Chemical Engineering and Mineral Processing*, vol. 8, pp. 167-182.

Haque, K.E. (1999) 'Microwave energy for mineral treatment processes – a brief review', *International Journal of Mineral Processing*, vol. 57, pp. 1–24.

Hayes, R.A., Price, D.M., Ralston, J., Smith, R.W. (1987) 'Collectorless flotation of sulphide minerals', *Mineral Processing and Extractive Metallurgy Review*, vol. 2, no. 3, pp. 203-234.

Hayes, R.A., Ralston, J. (1988) 'The collectorless flotation and separation of sulphide minerals by E_h control', *International Journal of Mineral Processing*, vol. 23, pp. 55-84.

Huang, Z., Li, W., Pan, Z., Liu, Y., Fang, M. (2013) 'High-temperature transformation of asbestos tailings by carbothermal reduction', *Clays and Clay Minerals*, vol. 61, no. 1, pp. 75-82.

Israelachvili, J. (2011) *Intermolecular and surface forces*, 3rd ed., Academic Press, London.

Kelebek, S., Tukel, C. (1999) 'The effect of sodium metabisulfite and triethylenetetramine system on pentlandite-pyrrhotite separation', *International Journal of Mineral Processing*, vol. 57, pp. 135-152.

Kelebek, S., Wells, P.F., Fekete, S.O. (1996) 'Differential flotation of chalcopyrite, pentlandite and pyrrhotite in Ni-Cu sulphide ores', *Canadian Metallurgical Quarterly*, vol. 35, no. 4, pp. 329-336.

Lu, Y., Zhang, M., Feng, Q., Long, T., Ou, L., Zhang, G. (2011) 'Effect of sodium hexametaphospate on separation of serpentine from pyrite', *Transactions of Nonferrous Metals Society of China*, vol. 21, pp. 208-213.

Masliyah, J., Czarnecki, J., Xu, Z. (2011) *Handbook on theory and practice of bitumen recovery from Athabasca oil sands*, Kingsley, Canada.

Merve Genc, A., Kilickaplan, I., Laskowski, J.S. (2012) 'Effect of pulp rheology on flotation of nickel sulphide ore with fibrous gangue particles', *Canadian Metallurgical Quarterly*, vol. 51, no. 4, pp. 368–375.

Minowa, T., Yoshikawa, M., Honshima, M. (1989) 'Improvement of the corrosion resistance on Nd-Fe-B magnet with nickel plating', *IEEE Transactions on Magnetics*, vol. 25, no. 5, pp. 3776–3778.

Moskalyk, R.R., Alfantazi, A.M. (2002) 'Nickel laterite processing and electrowinning practice', *Minerals Engineering*, vol. 15, pp. 593–605.

Mudd, G.M. (2010) 'Global trends and environmental issues in nickel mining: Sulfides versus laterites', *Ore Geology Reviews*, vol. 38, pp. 9–26.

Müller, P. (1994) 'Glossary of terms used in physical organic chemistry (IUPAC Recommendations 1994)', Pure and Applied Chemistry, vol. 66, no. 5, pp. 1077–1184.

Myers, D. (1999) *Surfaces, interfaces, and colloids: Principles and applications*, 2nd ed., John Wiley & Sons, New York.

nickel (Ni). (2014) In *Encyclopaedia Britannica*, Retrieved in 6 January 2014, <http://www.britannica.com/EBchecked/topic/414238/nickel>.

Niederhauser, M., Wisdom, T. (2013) 'The tailings evolution: Advancements, benefits, and challenges', *Proceedings of the Procemin 2013 10th*

International Mineral Processing Conference, Gecamin, Santiago, Chile, pp. 569.

Nishikawa, K., Takahashi, K., Karjalainen, A., Wen, C., Furuya, S., Hoshuyama, T., Todoroki, M., Kiyomoto, Y., Wilson, D., Higashi, T., Ohtaki, M., Pan, G.W., Wagner, G. (2008) 'Recent mortality from pleural mesothelioma, historical patterns of asbestos use, and adoption of bans: A global assessment', *Environmental Health Perspectives*, vol. 116, pp. 1675–1680.

Pollock, T.M., Tin, S. (2006) 'Nickel-based superalloys for advanced turbine engines: Chemistry, microstructure, and properties', *Journal of Propulsion and Power*, vol. 22, no. 2, pp. 361–374.

Rahilly, G., Price, N. (2003) 'Current products and practice Nickel allergy and orthodontics', *Journal of Orthodontics*, vol. 30, pp. 171–174.

Sedore, L. (2003) *MgO rejection from Birchtree ore at Inco's Manitoba division, Master of Engineering Thesis*, McGill University.

Uddin, S., Rao, S.R., Mirnezami, M., Finch, J.A. (2012) 'Processing an ultramafic ore using fiber disintegration by acid attack', *International Journal of Mineral Processing*, vol. 102-103, pp. 38–44.

Wei, Z., Fusheng, Y., Yuangang, L., Jianlin, Q., Anning, Z. (2011) 'Influence of microwave treatment under a hydrogen or methane atmosphere on the flotability of the macerals in Shenfu coals', *Mining Science and Technology (China)*, vol. 21, pp. 761–766.

Xu, M., Dai, Z., Dong, J., Ford, F., Lee, A. (2010) 'Fibrous minerals in ultramafic

    nickel sulphide ores', *Proceedings of the 49th annual conference of*

    metallurgists, Met Soc, Vancouver, British Columbia, Canada, pp. 223–

    235.

Zhang, Q., Wu, M., Zhao, W. (2005) 'Electroless nickel plating on hollow glass

    microspheres', *Surface and Coatings Technology*, vol. 192, pp. 213–219.

Chapter 2 Experimental Techniques

2.1 Zetaphoremeter

Zeta potential distributions were measured using Zetaphoremeter IV (CAD Instruments, France). This instrument measures the zeta potential of colloid particles in a suspension by electrophoresis techniques. Electrophoresis is a process where suspended particles in a liquid medium move under an applied electric field (Fuerstenau and Pradip, 2005). Zetaphoremeter IV employs a sophisticated image analysis which computes the electrophoretic mobility of colloid particles. Electrophoretic mobility is defined as the velocity of the colloid particles during electrophoresis divided by the electric field strength (Alvarez-Silva, 2011). The system outputs the histogram of zeta potential distributions calculated from electrophoretic mobility measurements using the Smoluchowski equation (Fuerstenau and Pradip, 2005; Masliyah et al., 2011).

Zeta potential distribution measurements have been used to study the interactions between two different particles by comparing the zeta potential distribution of the single particle system and that of the binary mixture system (Liu et al., 2002; Liu et al., 2004a; 2004b; 2005; Xu et al., 2003). Figure 2-1 shows the schematic illustrations of the zeta potential distribution measurements technique in analyzing the interactions between valuable and gangue mineral particles in a binary system. As shown in Figure 2-1a, the suspensions of valuable and gangue minerals each gives an individual zeta potential distribution with corresponding peaks at ζ_V and ζ_G. When the valuable and gangue minerals are mixed under

similar conditions, the zeta potential distributions of the binary mixture depend on the interactions between the valuable and gangue minerals. If there is no interaction between the two types of mineral, a bimodal zeta potential distribution with two peaks centered at almost the same position of the individually measured zeta potential distributions of each type of minerals is anticipated (Figure 2-1b). If there is a strong attraction between the valuable and gangue minerals, a single zeta potential distribution will be observed (Figure 2-1c and Figure 2-1d). The position of the peak depends on the ratio between the two types of mineral. In the case of weak attraction between the valuable and gangue minerals, a bimodal zeta potential distribution is anticipated as shown in Figure 2-1e.
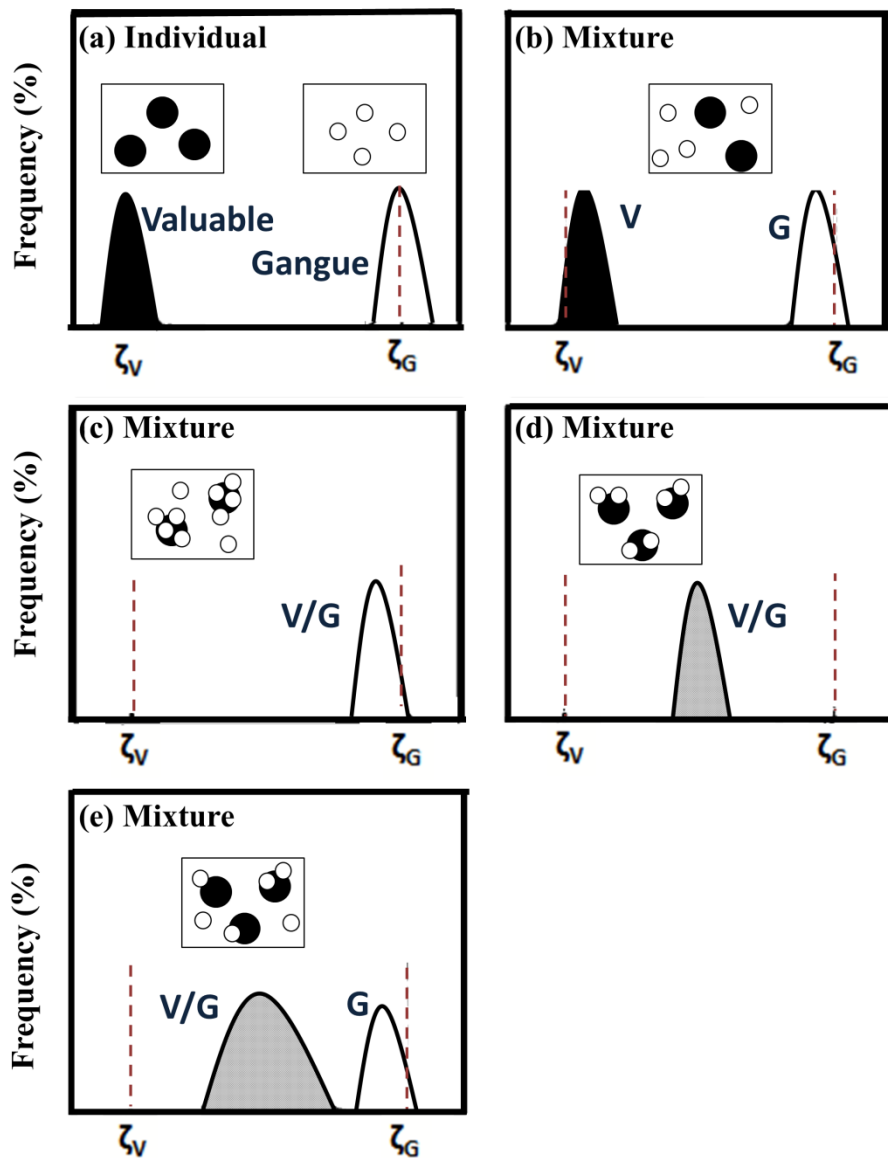
Figure 2-1 Schematics of zeta potential distributions, illustrating: (a) the individual zeta potential distributions of valuable and gangue minerals, (b) the binary mixture with no attraction, (c) strong attraction in the binary mixture (valuable mineral is fully coated with gangue mineral), (d) strong attraction in the binary mixture (valuable mineral is partially coated with insufficient amount of gangue mineral), and (e) weak attraction in the binary mixture (valuable mineral

is partially coated with some amount of gangue mineral unattached). The figures

are adapted from Liu et al. (2002).

2.2 Atomic force microscope (AFM)

The atomic force microscope (AFM) is a type of scanning probe microscopes, which has been developed since the invention of scanning tunneling microscope (STM) in the eighties (Binnig and Rohrer, 1983). The development of AFM allowed the imaging of both conducting and insulating surfaces (Binnig et al., 1986). Having small contact areas in its analysis, AFM technique reduces the detrimental issue of surface roughness and contamination (Butt et al., 2005).

Figure 2-2 shows an illustration of the working principle of an AFM for colloidal force measurement as well as topography imaging in this study. As shown in Figure 2-2a, a mineral substrate is scanned by a silicon nitride (Si_3N_4) AFM tip mounted to a cantilever spring. The deflection of the cantilever is detected by a photo-detector which monitors the reflection of a laser light from the cantilever. At a large separation distance (Figure 2-2b:a), there is zero deflection or zero force between the tip and the mineral surface. As the tip moves closer towards the surface, an increase or a decrease in the deflection output signal can be expected. An increasing deflection output signal corresponds to the repulsion between the two surfaces, indicated by the cantilever being deflected away from the mineral surface. A decreasing deflection output signal corresponds to the attraction between the two surfaces, indicated by the cantilever being deflected towards the mineral surface. Figure 2-2b:b indicates the repulsive case. Further moving the tip

towards the surface will eventually lead to the contact of the tip on the mineral surface (Figure 2-2b:c). During the retraction of the tip away from the mineral surface, the retracting deflection signal will be identical to the approaching signal if the interaction force between the tip and the surface is purely repulsive. If there is an adhesion between the tip and the mineral surface, the adhesive force will hold the tip on the surface as the cantilever retracts away from the surface. In this case, the deflection output signal follows the red line in Figure 2-2b. The tip will detach from the mineral surface when the restoring force during retraction exceeds the adhesive force; the deflection output signal returns to zero value. The topographic image of the sample can be obtained from the deflection of the cantilever and its position/location with respect to the sample (Butt et al., 2005). Knowing the spring constant of the cantilever, the deflection of the cantilever can also be translated into the force acting between the AFM tip and mineral substrate. More detailed descriptions of the interaction force measurements using an AFM can be found elsewhere (Ducker et al., 1991; 1992).

Photo-detector

Laser Source

Si_3N_4 tip → **Cantilever**

Mineral

(a)

Deflection

c

Repulsion

b

a

Piezo Height

Attraction

(b)
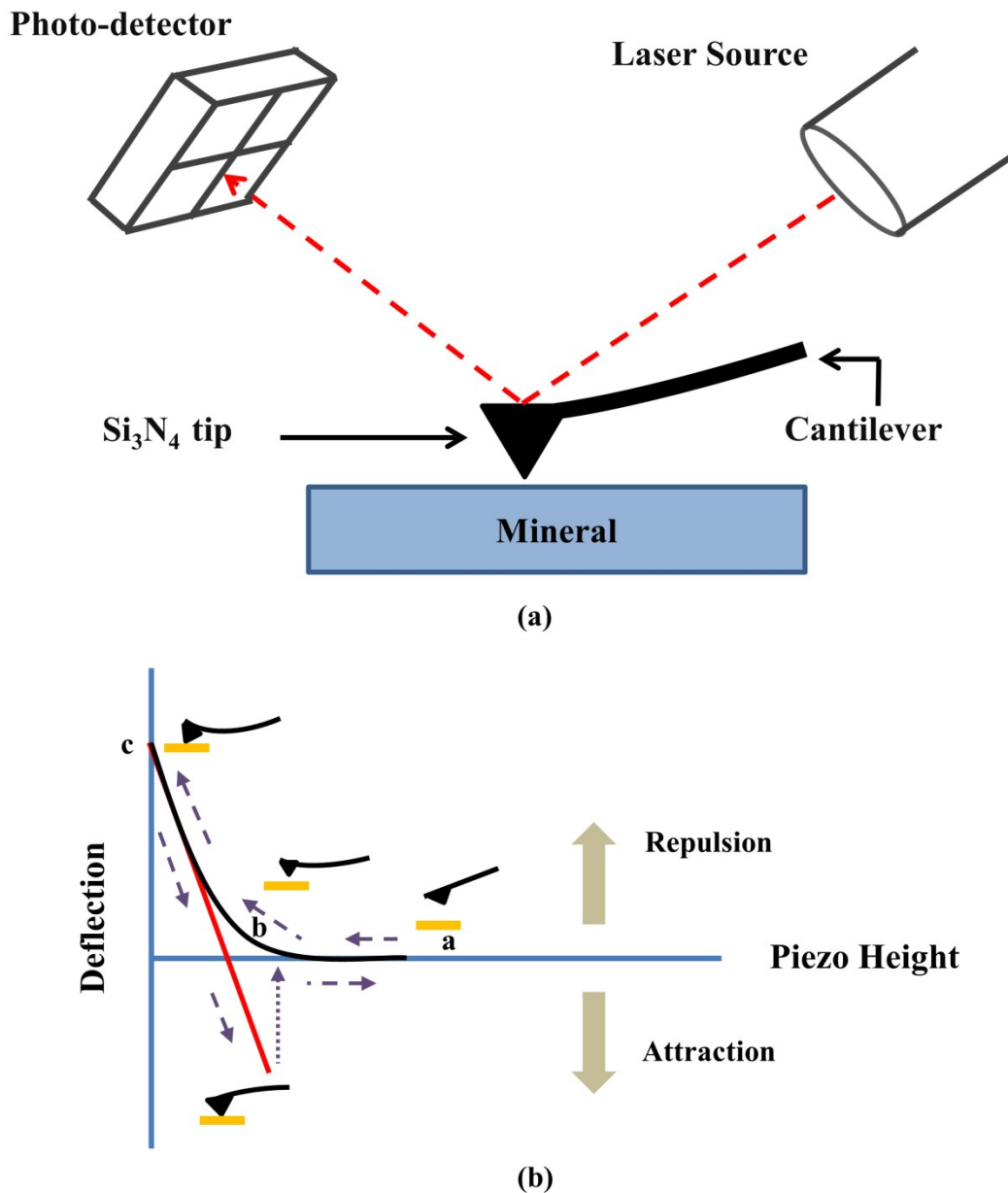
Figure 2-2 Schematic of working principle of an AFM.

2.3 Contact angle

Contact angle measurement is a common method in measuring the hydrophobicity of a solid surface. Contact angle is an important parameter in many industrial

processes, such as: mineral flotation, lubrication, liquid coating, printing, and oil recovery (Chau et al., 2009; Yuan and Lee, 2013). The contact angle is defined as the angle formed by the intersection of the liquid-vapor interface and the liquid-solid interface (Yuan and Lee, 2013), as illustrated in Figure 2-3.
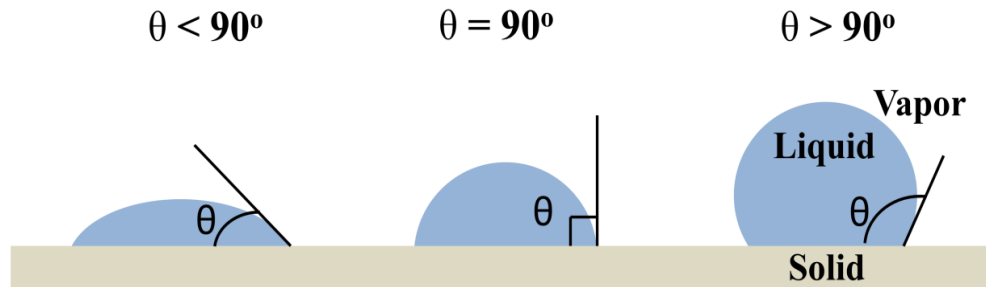
Figure 2-3 Schematic of contact angle formed by liquid droplets on a substrate.

One problem in a real mineral surface is that this surface is composed of both hydrophobic and hydrophilic domains (Rao and Leja, 2004). However, the contact angle measurements continue to show a correlation between flotation recovery and hydrophobicity as discussed in other literatures (Holuszko et al., 2008; Osasere, 2000).

2.4 Induction time apparatus

The air bubble-valuable mineral attachment is a prominent process in the successful mineral flotation. Thinning and rupture of the wetting film between the air bubble and mineral surface leads to the attachment of air bubble on mineral surface (Su et al., 2006). Induction time is defined as the minimum time required for the film to drain to a critical thickness and rupture spontaneously to form a

stable three phase contact line leading to an air bubble-particle aggregate (Yoon and Yordan, 1991). Induction time is a measure of hydrophobicity of a solid surface. Figure 2-4 shows the schematic of an induction time apparatus used in this study. The approach and retraction of an air bubble is controlled by applying a voltage to a speaker. The air bubble is generated at the end of a glass capillary tube (ID = 0.89 mm and OD = 1.33 mm) using a Gilmont micro-syringe. A CCD camera assists in viewing the positioning and contacting process between the air bubble and particles or substrate.
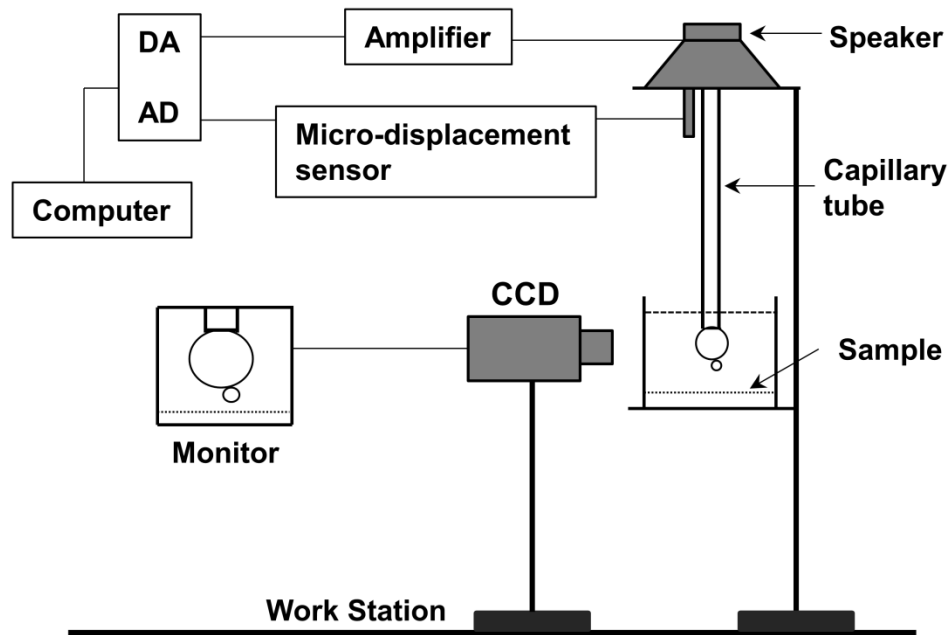
Figure 2-4 Schematic of the induction time apparatus.

2.5 Modified Hallimond tube

The flotation tests in this study were performed by using a modified Hallimond tube, as illustrated in Figure 2-5. The tube contains two parts. The top part (Figure 2-5a) consists of a vertical flotation tube and a concentrate bulb. The lower part

(Figure 2-5b) consists of a glass chamber with a sintered glass frit base with 1.6 μm pore size and a gas inlet. A magnetic stirring bar is placed in the lower part component to agitate the flotation pulp. A nitrogen gas flows into the tube through the gas inlet, with a pre-set gas flow rate using a flow-meter.

Concentrate bulb

Flotation tube

Glass frit

(a)　　　　(b)
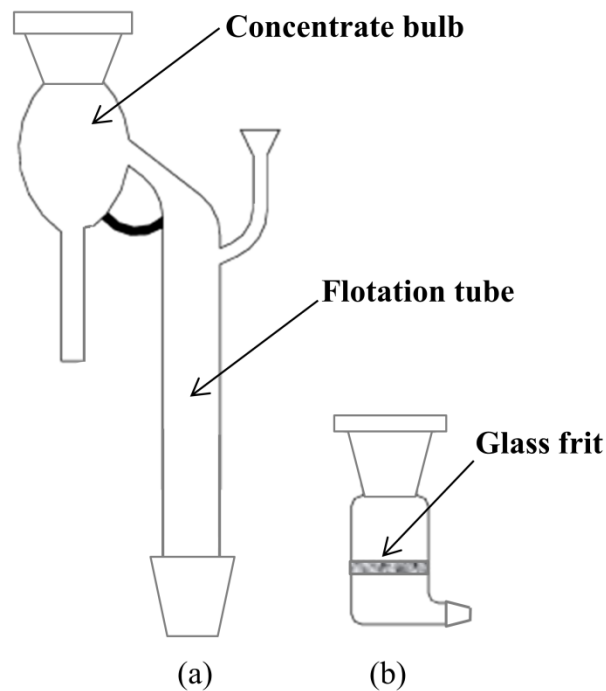
Figure 2-5 Schematic of a modified Hallimond tube: (a) top and (b) bottom parts.

2.6 Scanning electron microscope

Scanning electron microscope (SEM) enables the characterization of sample's morphology at high resolution and high magnification. A focused beam of electrons, typically generated from a tungsten filament, is accelerated through a system of apertures and electromagnetic lenses, which scans the surface of a

sample. The signals produced by the electron-sample interaction reveal information such as: morphology and elemental analysis.

For chemical analysis purpose, SEM may be coupled with Auger electron spectroscopy (AES) and energy dispersive X-Ray spectroscopy (EDX). In AES, the sample is irradiated with a high energy primary electron beam (2-10 keV). The irradiation results in the emission of Auger electrons. The emitted Auger electrons correspond to the characteristics of the elements present on the sample surface. The depth of analysis in AES is between 3-5 nm. In EDX, a high energy primary electron beam is also utilized to irradiate the sample surface, which then results in X-ray emission. The X-ray emission allows the measurement of the elemental composition in a sample surface. The typical depth of analysis in EDX is between 1-3 μm.

2.7 References

Alvarez-Silva, M. (2011) *Surface chemistry study on the pentlandite-serpentine system, PhD Dissertation*, McGill University.

Binnig, G., Rohrer, H. (1983) 'Scanning Tunneling Microscopy', *Surface Science*, vol. 126, pp. 236–244.

Binnig, G., Quate, C.F., Gerber, C. (1986) 'Atomic Force Microscope', *Physical Review Letters*, vol. 56, no. 9, pp. 930–933.

Butt, H.J., Cappella, B., Kappl, M. (2005) 'Force measurements with the atomic force microscope: Technique, interpretation and applications', *Surface Science Reports*, vol. 59, pp. 1–152.

Chau, T.T., Bruckard, W.J., Koh, P.T.L., Nguyen, A.V. (2009) 'A review of factors that affect contact angle and implications for flotation practice', *Advances in Colloid and Interface Science*, vol. 150, pp. 106–115.

Ducker, W.A., Senden, T.J., Pashley, R.M. (1991) 'Direct measurement of colloidal forces using an atomic force microscope', *Nature*, vol. 353, no. 6341, pp. 239–241.

Ducker, W.A., Senden, T.J., Pashley, R.M. (1992) 'Measurement of forces in liquids using a force microscope', *Langmuir*, vol. 8, no. 7, pp. 1831–1836.

Fuerstenau, D.W., Pradip. (2005) 'Zeta potentials in the flotation of oxide and silicate minerals', *Advances in Colloid and Interface Science*, vol. 114-115, pp. 9–26.

Holuszko, M.E., Franzidis, J.P., Manlapig, E.V., Hampton, M.A., Donose, B.C., Nguyen, A.V. (2008) 'The effect of surface treatment and slime coatings on ZnS hydrophobicity', *Minerals Engineering*, vol. 21, pp. 958–966.

Liu, J., Zhou, Z., Xu, Z., Masliyah, J. (2002) 'Bitumen-clay interactions in aqueous media studied by zeta potential distribution measurement', *Journal of Colloid and Interface Science*, vol. 252, pp. 409–418.

Liu, J., Xu, Z., Masliyah, J. (2004a) 'Interaction between bitumen and fines in oil sands extraction system: implication to bitumen recovery', *The Canadian Journal of Chemical Engineering*, vol. 82, no. 4, pp. 655–666.

Liu, J., Xu, Z., Masliyah, J. (2004b) 'Role of fine clays in bitumen extraction from oil sands', *AIChE Journal*, vol. 50, no. 8, pp. 1917–1927.

Liu, J., Xu, Z., Masliyah, J. (2005) 'Interaction forces in bitumen extraction from oil sands', *Journal of Colloid and Interface Science*, vol. 287, no. 2, pp. 507–520.

Masliyah, J., Czarnecki, J., Xu, Z. (2011) *Handbook on theory and practice of bitumen recovery from Athabasca oil sands*, Kingsley, Canada.

Osasere, O.F. (2000) 'Relation of contact angle data to Hallimond tube flotation of coal with coagulants and flocculants', *Fuel*, vol. 79, pp. 193–199.

Rao, S.R., Leja, J. (2004) *Surface chemistry of froth flotation*, Kluwer Academic Publishers, New York, USA.

Su, L., Xu, Z., Masliyah, J. (2006) 'Role of oily bubbles in enhancing bitumen flotation', *Minerals Engineering*, vol. 19, pp. 641–650.

Xu, Z., Liu, J., Choung, J.W., Zhou, Z. (2003) 'Electrokinetic study of clay interactions with coal in flotation', *International Journal of Mineral Processing*, vol. 68, pp. 183-196.

Yoon, R.H., Yordan, J.L. (1991) 'Induction time measurements for the quartz-amine flotation system', *Journal of Colloid and Interface Science*, vol. 141, no. 2, pp. 374-383.

Yuan, Y., Lee, T.R. (2013) 'Contact angle and wetting properties', In Bracco, G. & Holst, B. (eds.), *Surface Science Techniques*, pp. 3–34, Springer-Verlag Berlin Heidelberg.

Chapter 3 Understanding Interaction Mechanisms between Pentlandite and Gangue Minerals by Zeta Potential and Surface Force Measurements[1]

3.1 Introduction

Nickel has been widely used in many engineering applications (e.g. stainless steel, shape memory alloys) and plays an important role in the production of wear and corrosion resistant materials (Minowa et al., 1989; Rahilly and Price, 2003; Zhang et al., 2005). Due to the declining reserve of high-grade nickel ores, the low-grade ultramafic nickel ores (e.g. Thompson Pipe deposit, Manitoba, Canada) have been revisited and are becoming important resources of nickel mineral (Dai et al., 2009; Merve Genc et al., 2012). However, most of these ultramafic nickel ores have low nickel grade and high magnesia (MgO) content, leading to challenging issues during the flotation process.

The MgO-containing minerals in the low-grade nickel ores mainly include serpentine and olivine. Serpentine has a layered structure which is comprised of 1:1 layering of one silica (SiO_4) tetrahedral layer bonded to a brucite (Mg-O) octahedral layer (Mookherjee and Stixrude, 2009). The tetrahedral and octahedral layers are held together by van der Waals forces (Alvarez-Silva et al., 2010). Serpentine group consists of three common polymorphs: chrysotile, antigorite, and lizardite. Chrysotile is a fibrous, tubular mineral and classified as asbestos (Zussman, 1978). In contrast, lizardite has a flat-layered and platy structure while

---

[1] A version of this chapter was submitted for publication on *Minerals Engineering* journal.

antigorite has a curved, corrugated sheet structure (Zussman, 1978). As opposed to serpentine, olivine is an orthosilicate mineral consisting of isolated SiO_4 tetrahedral connected via divalent cations (i.e. magnesium and iron) in six fold coordination and it has no layered structure (Gualtieri et al., 2003).

The challenging issues during the processing of such low-grade ores mainly include the high pulp viscosity and slime coating on the valuable nickel bearing mineral (i.e. pentlandite), which significantly reduce nickel recovery and grade concentrate during flotation (Feng et al., 2012b; 2013). The high pulp viscosity is attributed to the high-serpentine content in the low-grade ultramafic nickel ore (Dai et al., 2009). Hence, the flotation and grinding can only be done at low percent solids, which largely increase the operation cost. The presence of fibrous minerals (eg. chrysotile) is responsible for the formation of air bubble-macro fibres aggregates, which easily report to the flotation concentrate and lead to the recovery of MgO-containing minerals (Xu et al., 2010).

The slime coating on pentlandite surface is mainly due to the presence of serpentine. The interaction between serpentine and pentlandite has been discussed in previous studies (Bremmel et al., 2005; Edwards et al., 1980). The occurrence of slime coating is directly related to the surface potentials of pentlandite and serpentine. The formation of slime coating is mainly attributed to the attractive interaction between a positively charged serpentine and a negatively charged pentlandite. Partial slime coating normally leads to the dilution of the flotation concentrate, while the loss of nickel recovery occurs when heavily coated pentlandite becomes hydrophilic (Alvarez-Silva, 2011). In addition, the presence

of serpentine in the nickel concentrate results in the imposition of smelter penalties for mineral processing companies due to higher slag melting point (Alvarez-Silva, 2011; Feng et al., 2012b; 2013).

Thermal pretreatment of the ultramafic nickel ores is being investigated as a way to improve flotation by reducing or eliminating the negative effects of serpentine (Bobicki et al., 2014). It is known that serpentine transforms into olivine at above the dehydroxylation temperature (Gualtieri et al., 2012; Huang et al., 2013; Leonelli et al., 2006). In another aspect of flotation, sodium carbonate is also widely used in nickel ore processing to control the precipitation of magnesium hydroxide by sequestering magnesium to form magnesite (Alvarez-Silva, 2011).

Therefore, a better understanding of the interaction between valuable nickel mineral (i.e. pentlandite) with gangue minerals (i.e. serpentine, olivine, and magnesite) has a practical importance for the flotation of low-grade ultramafic nickel ores. Zeta potential distribution measurement proves to be a powerful technique to study slime coating in a colloidal system, which has been shown for bitumen-clay and coal-clay interactions (Liu et al., 2002; Liu et al., 2004a; 2004b; 2005; Xu et al., 2003). The interaction in a binary mixture can be inferred based on the shift of the zeta potential distribution of the mixture with respect to that of each individual component. AFM has also been used to directly measure surface forces between an AFM tip and the surfaces of clay minerals (Gupta and Miller, 2010; Yan et al., 2011). Surface properties of the minerals (e.g. surface charges, surface potential) could be inferred from the force-distance profiles. In this study, the interaction between pentlandite and gangue minerals such as serpentine,

olivine, and magnesite has been investigated using zeta potential distribution measurements. In addition, direct surface force measurement has been conducted on serpentine, olivine, and magnesite surfaces using a silicon nitride AFM tip. This study provides new insights into the interaction between pentlandite and gangue minerals in the flotation of low-grade nickel sulphide ore.

3.2 Experimental

3.2.1 Materials and reagents

Serpentine and olivine rocks were obtained from Ward's Natural Science Establishment. Magnesium carbonate powder (Fisher Scientific), magnesite rock (Minerals Unlimited, USA), and Min-u-sil 5 silica (US Silica, USA) were used as received. Pentlandite was obtained from Vale Base Metals Technology Development (Mississauga, Ontario, Canada). Serpentine and olivine were crushed and pulverized to obtain the -200 μm size fraction. Serpentine, olivine, and pentlandite samples were then sieved to obtain the -38 μm size fraction to be used for the zeta potential distribution measurement. Some of the serpentine, olivine, and magnesite rocks were kept for the AFM force measurement. Pentlandite was washed using 0.1 M hydrochloric acid and deionized water, followed by freeze drying and stored in the -20 $^{\circ}$C freezer before zeta potential experiments.

Hydrochloric acid (HCl) and potassium hydroxide (KOH) from Fisher Scientific were used as pH modifiers. Potassium chloride (KCl) from Fisher Scientific was used for the preparation of supporting electrolyte solution. All the reagents used

were of ACS reagent grade. Deionized water (Milli-Q water) with a resistivity of 18.2 MΩ cm prepared with Millipore Elix 5 purification system was used throughout this study.

3.2.2 Thermogravimetry analysis

A Q500 series thermogravimetry (TG) instrument (TA Instrument) was used in this study. Powdered serpentine sample was placed in an open-type platinum pan. The heating rate was set to 10 ^{o}C/min. The measurement was performed under nitrogen atmosphere. The balance and sample purge gas flow rate were set to 40 mL/min.

3.2.3 Zeta potential distribution measurements

3.2.3.1 Suspension preparation

For the single mineral measurement, the suspension was prepared by adding the mineral in the supporting electrolyte solution (10 mM KCl). The suspension of serpentine, olivine, and magnesite were stirred for 24 hours prior to the measurement. Pentlandite suspension was prepared fresh prior to the measurement to limit oxidation. Prior to the measurement, the pH of the suspension was adjusted and the suspension was then sonicated for 5 minutes.

In the case of a binary mineral mixture suspension, the prepared mineral suspensions were mixed at a 1:1 solid ratio. Prior to the measurement, the pH of the suspension was adjusted to 10.1 and the suspension was then sonicated for 5 minutes. The pH 10.1 was selected based on the operational conditions at the Thompson Mill (Dai et al., 2009).

3.2.3.2 Zeta potential distribution measurements technique

The zeta potential distribution measurements were performed on the single and the mixed mineral systems. The zeta potential distributions were measured based on the electrophoretic method using a Zetaphoremeter IV CAD Instruments equipped with a rectangular electrophoresis cell, a pair of hydrogenated palladium electrodes, a laser illuminator, and a CCD camera. The system allows for an accurate positioning of the stationary layer, where the electrophoretic mobility can be measured accurately. The built-in imaging processing software traces the movement of 50-100 particles in the stationary layer, 5 times in each direction by alternating positive and negative electrode potentials. The electrophoretic mobility distribution is then converted to zeta potential distribution by using Smoluchowski equation (Masliyah et al., 2011).

3.2.4 AFM force measurements

3.2.4.1 Preparation of mineral surfaces

The rock pieces of serpentine, olivine, and magnesite minerals were mounted in an epoxy resin (West System Inc., Bay City, MI, USA). The samples were then polished to obtain flat mineral surface. A wet grinding using 45 µm grinding paper was performed, followed by series of polishing using diamond slurry (9 µm and 3 µm) and alumina slurry (0.05 µm). The samples were then washed and sonicated in Milli-Q water to remove the slurry suspension residue. For AFM measurements, the samples were rinsed with Milli-Q water, and then subjected to

a high-pressure nitrogen gas blow before immersed in a desired electrolyte solution.

3.2.4.2 AFM force measurements

A MFP-3D atomic force microscope (Asylum Research) was used in this study. Silicon nitride tip (PNP, Nano World AG, Switzerland, 17 kHz resonant frequency, 20 nm tip radius) was used for obtaining AFM images and force profiles. The tip geometry was examined using a field emission scanning electron microscope (FE-SEM) (JAMP-9500F, Jeol, Japan). The force measurements were carried out in 1 mM KCl solutions at pH 10.1. The tip-mineral substrate in the aqueous solution system was allowed to stabilize for at least 30 minutes before the force measurements were performed. Topographical images of the mineral surfaces were obtained using the contact mode on the AFM. The interaction forces were measured for at least three times at various locations where the roughness was less than 1 nm over 0.5 x 0.5 μm^2 area. All of the experiments were conducted at room temperature. The raw force profiles were analyzed by IgorPro software which converts the deflection-distance data to force-distance curve. The interaction force profiles were fitted by using the DLVO theory for the conical tip-flat substrate system, where the total interaction force (F^{DLVO}) includes the electrostatic double layer force (F^{edl}) and van der Waals forces (F^{vdw}) as given by (Drelich et al., 2007; Yan et al., 2011):

Electrostatic double layer force of constant surface potential:

$$F^{edl} = 4\pi\varepsilon_o\varepsilon\Psi_T\Psi_S(\alpha_o e^{-\kappa D} - \alpha_1 e^{-\kappa L_1}) + 2\pi\varepsilon_o\varepsilon(\Psi_T^2 + \Psi_S^2)(\alpha_2 e^{-2\kappa D} -$$

$$\alpha_3 e^{-2\kappa L_2}) + \frac{4\pi\varepsilon_o\varepsilon\kappa}{\tan\alpha}\left[b_1\Psi_T\Psi_S e^{-\kappa L_1} + b_2\frac{(\Psi_T^2 + \Psi_S^2)}{2}e^{-2\kappa L_1}\right] \quad (3.1)$$

Electrostatic double layer force of constant surface charge density:

$$F^{edl} = \frac{4\pi}{\varepsilon_o\varepsilon\kappa^2}\sigma_T\sigma_S(\alpha_o e^{-\kappa D} - \alpha_1 e^{-\kappa L_1}) + \frac{2\pi}{\varepsilon_o\varepsilon\kappa^2}(\sigma_T^2 + \sigma_S^2)(\alpha_2 e^{-2\kappa D} -$$

$$\alpha_3 e^{-2\kappa L_2}) + \frac{4\pi}{\varepsilon_o\varepsilon\kappa^2\tan\alpha}\left[b_1\sigma_T\sigma_S e^{-\kappa L_1} + b_2\frac{(\sigma_T^2 + \sigma_S^2)}{2}e^{-2\kappa L_1}\right] \quad (3.2)$$

Van der Waals forces:

$$F^{vdw} = \frac{A_{132}}{6}\left[\frac{(R+D)-2L_1}{L_1^2} - \frac{R-D}{D^2}\right] - \frac{A_{132}}{3\tan^2\alpha}\left(\frac{1}{L_1} + \frac{R\sin\alpha\tan\alpha - D - R(1-\cos\alpha)}{L_1^2}\right) \quad (3.3)$$

where,

$$L_1 = D + R(1 - \cos\alpha); \; \alpha_o = \kappa R - 1; \; \alpha_1 = \kappa R\cos(\alpha - 1); \; \alpha_2 = \alpha_o + 0.5;$$

$$\alpha_3 = \alpha_1 + 0.5$$

$$b_1 = R\sin\alpha - \frac{D + R(1 - \cos\alpha)}{\tan\alpha} + \frac{1}{\tan\alpha}\left[L_1 + \frac{1}{\kappa}\right]$$

$$b_2 = R\sin\alpha - \frac{D + R(1 - \cos\alpha)}{\tan\alpha} + \frac{1}{\tan\alpha}\left[L_1 + \frac{1}{2\kappa}\right]$$

The subscripts S and T refer to the substrate and the tip, respectively. The symbols α and β refer to the geometrical angles of the tip as illustrated in Figure 3-1, with $\alpha + \beta = 90^o$. D is the distance between the substrate and the end of the tip; L is the distance between the substrate and the differential surface section of the tip; R is the radius of the spherical cap at the end of the tip; r is the radius of the circle of the tip at a given vertical location; ε and ε_o are the permittivity of the solution and vacuum, respectively; κ^{-1} is the Debye length; and A_{132} is the combined Hamaker

constant of the tip-solution-substrate system. The surface potential (Ψ) and the surface charge density (σ) are correlated to each other by the Grahame equation (Israelachvili, 2011; Masliyah and Bhattacharjee, 2006):

$$\sigma = \sqrt{8 c_o \varepsilon \varepsilon_o k_B T} \sinh\left(\frac{e\Psi}{2 k_B T}\right) \tag{3.4}$$

where c_o is the bulk ion number electrolyte concentration; k_B is the Boltzmann constant; e is the elementary charge; and T is temperature in Kelvin.
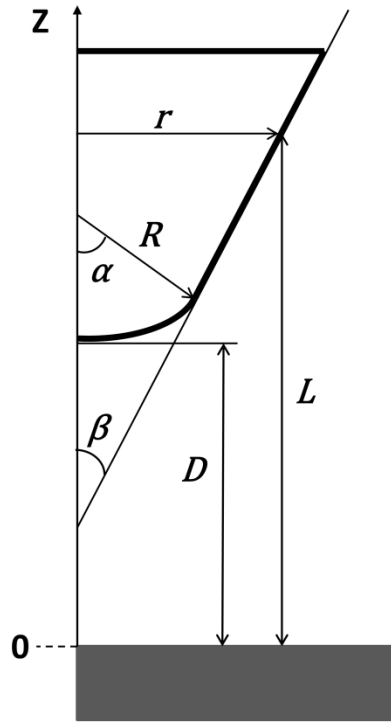
Figure 3-1 Geometrical illustration of the conical AFM tip with spherical apex interacting with a flat substrate.

The Hamaker constant for two identical objects interacting in vacuum (A_i) is given by the following equation (Israelachvili, 2011):

$$A_i = \frac{3}{4} k_B T \left(\frac{\varepsilon_i - 1}{\varepsilon_i + 1}\right)^2 + \frac{3h\nu_v}{16\sqrt{2}} \frac{(n_i^2 - 1)^2}{(n_i^2 + 1)^{1.5}} \tag{3.5}$$

where ε_i is the static dielectric constant for material I; n_i is the refractive index of material I; h is the Planck's constant; and ν_v is the main absorption frequency in the UV region. The data for each material are given in Table 3-1.

Table 3-1 The values used in the calculation of Hamaker constant A taken from literature.

Materials	Dielectric constant (ε_i)	Refractive index (n_i)	Reference
Serpentine	11.48	1.56	Rosenholtz and Smith, 1936; Mooney and Knacke, 1985
Olivine	6.77	1.67	Rosenholtz and Smith, 1936; Game, 1941
Magnesite	6.99	1.70	Rosenholtz and Smith, 1936; Baas-Becking and Galliher, 1931
Silica	3.82	1.448	Bergström, 1997
Silicon nitride	7.4	1.988	Bergström, 1997
Water	78.5	1.333	Yan et al., 2013

The Hamaker constant for two different materials (1 and 2) interacting across a solution (3) is given by the following equation (Faghihnejad and Zeng, 2012; Zeng, 2013):

$$A_{132} = \left(\sqrt{A_{11}} - \sqrt{A_{33}}\right)\left(\sqrt{A_{22}} - \sqrt{A_{33}}\right) \tag{3.6}$$

3.3 Results and discussion

3.3.1 Thermal characteristic of serpentine

The TG analysis was performed to understand the thermal properties of the serpentine used in this study. Figure 3-2 shows the typical TG profile obtained from heating serpentine mineral under nitrogen atmosphere from room temperature to 1000 ^{o}C. A small, gradual mass loss (~ 2%) was observed from room temperature to around 450 ^{o}C (Figure 3-2), which can be ascribed to the loss of physically absorbed water (Viti, 2010). A significant mass loss (~ 13%) was observed between 550-800 ^{o}C (Figure 3-2), which is due to the dehydroxylation (Viti, 2010). Consistent with previous observations (Brindley and Hayami, 1964; Cattaneo et al., 2003; Viti, 2010), the dehydroxylation starts at about 550 ^{o}C according to equation 3.7:

$$Mg_3Si_2O_5(OH)_4 \rightarrow Mg_3Si_2O_7 + 2H_2O \tag{3.7}$$

and completes around 800 ^{o}C where nucleation and growth of forsterite (olivine) occurs according to equation 3.8:

$$2Mg_3Si_2O_7 \rightarrow 3Mg_2SiO_4 + SiO_2 \tag{3.8}$$

Theoretically, the dehydroxylation and conversion to olivine causes a total mass loss of 13%, consistent with the TG measurement.
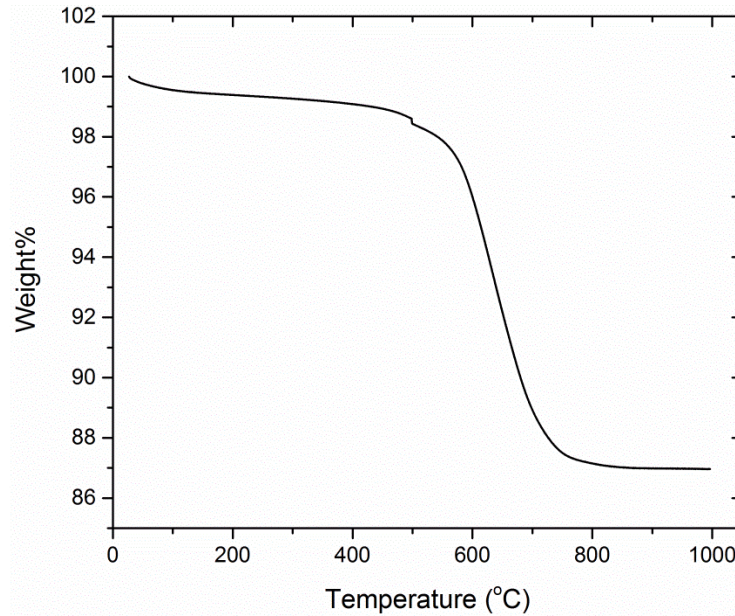
Figure 3-2 TG analysis of serpentine heated under nitrogen atmosphere.

3.3.2 Zeta potential distribution measurements of single mineral and binary mineral mixture

The zeta potential measurements were performed to characterize the surface charge properties of mineral particles and understand the interaction mechanisms among mineral particles, as presented in the following sections.

3.3.2.1 Zeta potential of single minerals as a function of pH

The zeta potential of single mineral suspensions (i.e., serpentine, olivine, magnesite, and pentlandite) was characterized in 10 mM KCl solution as a function of the solution pH, as shown in Figure 3-3. The zeta potential of serpentine (■) ranged from 43 to 50 mV between pH 4 to 9 and decreased to 30

mV at pH 10 and further to 20 mV at pH 10.4. This trend may indicate an isoelectric point (0 mV) for serpentine at pH higher than 11. For olivine (●), the zeta potential changed from positive (2 mV) at pH 2.4 to negative (-32 mV) at pH 10.5, and an isoelectric point was observed at pH 3. The zeta potential of magnesite (▲) was negative from pH 7 (-6 mV) to pH 10.7 (-10 mV). It is noted that the zeta potential measurement of magnesite could not be done below pH 7 due to high solubility of the mineral at pH<7. Similar to olivine, the zeta potential of pentlandite (★) changed from positive at low pH to negative at high pH, with a zeta potential of -11 mV at pH 10 and an isoelectric point at pH 3.8.

Based on the zeta potential measurement of individual mineral (Figure 3-3), the interaction between pentlandite and the three other minerals at pH 10.1 can be predicted. At this pH, pentlandite, olivine, and magnesite were all negatively charged, while serpentine was positively charged. Therefore, no strong electrostatic attraction is expected in the pentlandite-olivine and pentlandite-magnesite systems at pH 10.1 due to similar surface charges, while strong electrostatic attraction is expected in the pentlandite-serpentine system due to dissimilar surface charges.
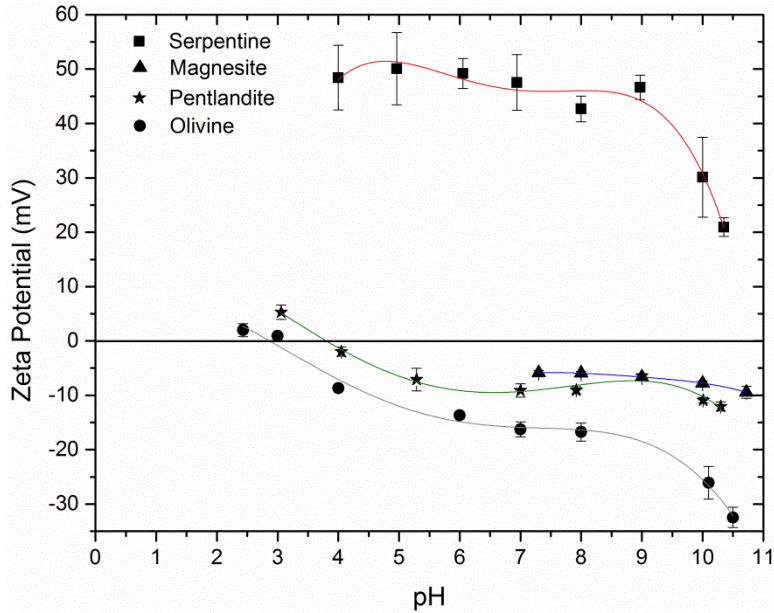
Figure 3-3 The zeta potential of different mineral suspensions as a function of pH in 10 mM KCl solution (■ – serpentine, ▲ – magnesite, ★ – pentlandite, ● – olivine).

3.3.2.2 Zeta potential distributions of single and binary minerals at pH 10.1

To understand the mineral interactions, the zeta potential distributions for the suspensions of individual mineral and binary mixture minerals were examined and compared at pH 10.1 in 10 mM KCl solution, including pentlandite-serpentine system (Figure 3-4), pentlandite-olivine system (Figure 3-5), and pentlandite-magnesite system (Figure 3-6). As shown in Figure 3-4a, the individual distribution peaks of pentlandite and serpentine were well separated and centered at -10 mV and 30 mV, respectively. The single distribution of zeta potential for the binary mixture of pentlandite and serpentine was centered at 18 mV (Figure 3-4b). The single distribution peak for the mixture indicated that a strong attraction happened between serpentine and pentlandite, with a partial

41

coverage of pentlandite surface with serpentine. The strong attraction between pentlandite and serpentine observed in this study is consistent with the previous findings (Bremmel et al., 2005; Edwards et al., 1980).
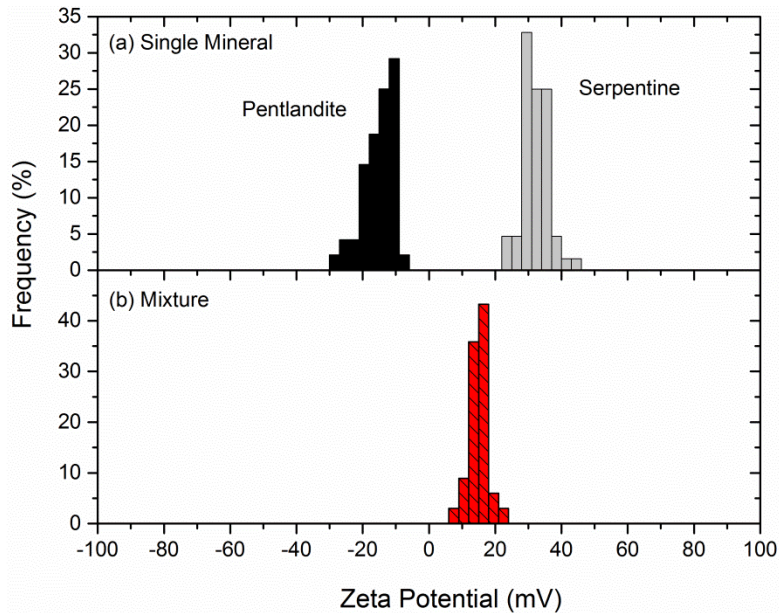
Figure 3-4 The zeta potential distributions for pentlandite and serpentine at pH 10.1 in 10 mM KCl solution: (a) individual suspensions and (b) binary mixtures.

For the pentlandite-olivine system, the individual distribution peaks of pentlandite and olivine were not far and centered at -10 mV and -28 mV, respectively (Figure 3-5a). The zeta potential distribution for the mixture of pentlandite and olivine showed a single distribution, however, with two distinct spikes centered at -20 mV and -12 mV (Figure 3-5b). Due to hydrodynamic interaction of moving particles at different electrophoretic mobilities, a shift of individual zeta potential distribution peaks towards each other may be observed in the mixture system (Liu et al., 2002). The shift of these individual peaks was represented as the two distinct peaks that almost coincided in the mixture zeta potential distribution in

Figure 3-5b. The two distinct spikes may indicate the repulsion between pentlandite and olivine.
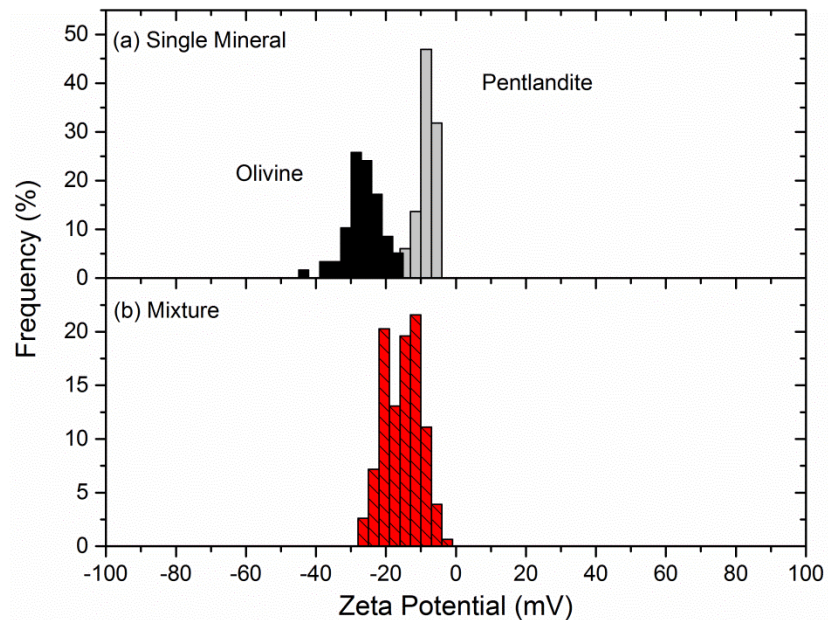
Figure 3-5 The zeta potential distributions for pentlandite and olivine at pH 10.1 in 10 mM KCl solution: (a) individual suspensions and (b) binary mixtures.

For the pentlandite-magnesite system, the individual distribution peaks of pentlandite and magnesite were very close and centered at -10 mV and -7 mV, respectively (Figure 3-6a). The zeta potential for the mixture of pentlandite and magnesite showed a single distribution with two distinct spikes centered at -14 mV and -7 mV (Figure 3-6b). In this mixture system, the hydrodynamic interaction was not significantly observed. This was possibly due to the mobility of the two minerals which were quite similar. The two distinct spikes may also be an indication of the repulsion between pentlandite and magnesite.
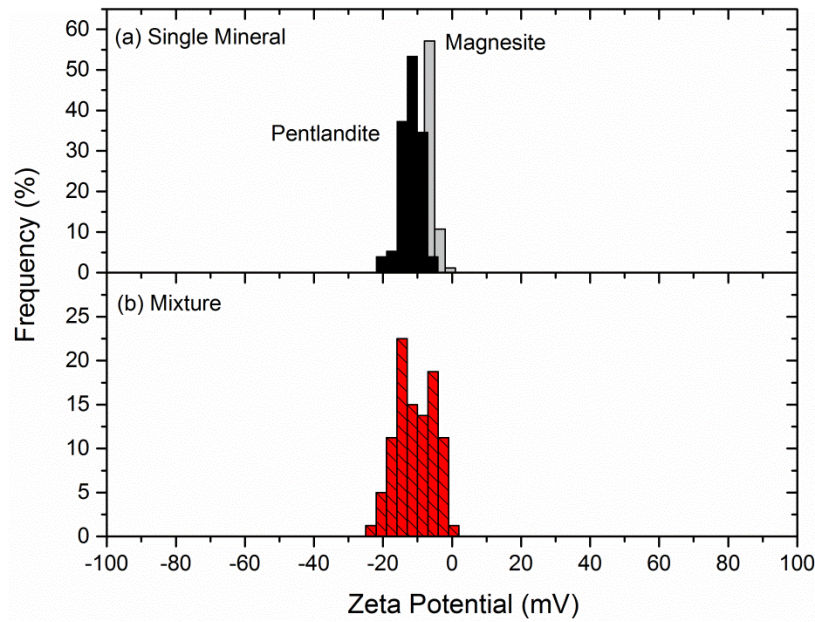
Figure 3-6 The zeta potential distributions for pentlandite and magnesite at pH 10.1 in 10 mM KCl solution (a) individual suspensions and (b) binary mixtures.

As a comparison, the zeta potential distribution of pentlandite-silica system at pH 10.1 in 10 mM KCl solution is also studied, as shown in Figure 3-7. The individual distribution peaks of pentlandite and silica were centered at -10 mV and -45 mV, respectively (Figure 3-7a). The mixture zeta potential showed two separate distributions; the left distribution was centered at -39 mV, while the right distribution was centered at -18 mV (Figure 3-7b). Due to hydrodynamic interaction, the silica and pentlandite peaks shifted towards each other as shown in the mixture distribution. The two separate distributions in the mixture indicated a marginal, or if there was any, attractive force between the two minerals.
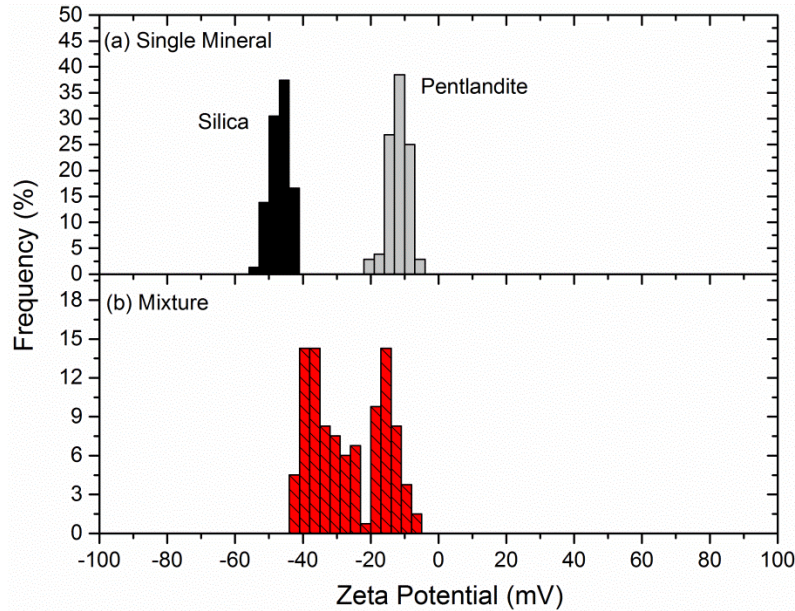
Figure 3-7 The zeta potential distribution for pentlandite and silica at pH 10.1 in 10 mM KCl solution (a) individual suspensions and (b) binary mixtures.

3.3.3 AFM force measurements

The zeta potential measurements provided important interaction information between valuable mineral (pentlandite) and gangue minerals (serpentine, olivine, magnesite). To provide complimentary proof and more information, AFM force measurements were performed to directly measure the interaction forces on different minerals. Considering the negative charge property of both silicon nitride and pentlandite at pH 10.1, silicon nitride AFM tip was selected to represent a negatively charged pentlandite surface to probe its interactions with gangue minerals (i.e., silicon nitride tip *vs.* serpentine, silicon nitride tip *vs.* olivine, silicon nitride tip *vs.* magnesite) at pH 10.1 in 1 mM KCl solution.

3.3.3.1 Characterization of the silicon nitride AFM tip

The characteristics (shape, chemical composition, surface charge) of the silicon nitride AFM tip was studied by FE-SEM, scanning Auger electron spectroscopy, and direct AFM force measurements between an AFM tip and a silicon wafer, as shown in Figure 3-8a, Figure 3-8b, and Figure 3-9, respectively. Figure 3-8a shows the pyramid-shaped silicon nitride tip used in this study. The scanning Auger electron spectrum shows the tip consists mainly of silicon and nitrogen with a small amount of oxygen, as indicated in Figure 3-8b.
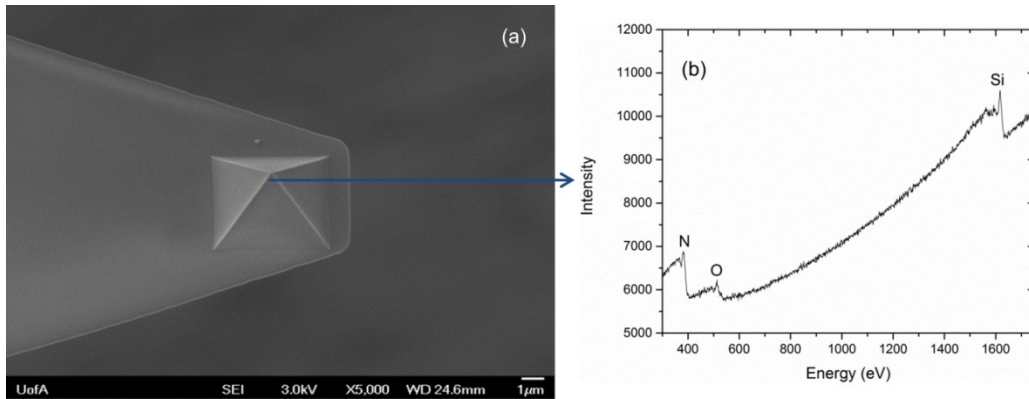
Figure 3-8 Characterization of the silicon nitride AFM tip: (a) the FE-SEM image and (b) the scanning Auger electron spectroscopy taken from the top end of the tip as indicated by the arrow line in the figure.

As the surface potential of silica has been well characterized at a given solution pH (Liu et al., 2003; Zhao et al., 2008), silica wafer was used as a reference substrate to determine the surface potential of the tip. By fitting the experimental force-distance profiles using the DLVO model, the surface potential of the silicon nitride AFM tip could be obtained. Figure 3-9 shows typical force-distance curve of a silicon nitride tip interacting with a silica wafer at pH 10.1 in 1 mM KCl solution. At pH 10.1, the approaching interaction force was purely repulsive.

Since the isoelectric point of silica is around pH 2 (Parks, 1965; 1967), the silica wafer can be considered as negatively charged, with surface potential of -65 mV at pH 10.1 (Zhao et al., 2008). The Hamaker constant for silica-water-silicon nitride tip was calculated to be 1.32×10^{-20} J, based on the data given in Table 3-1. By using the DLVO model, the surface potential of the tip was estimated to be -82 mV, which is comparable to the previous reports. (-85 mV from Yan et al., 2011; and -82 mV from Yin and Drelich, 2008).
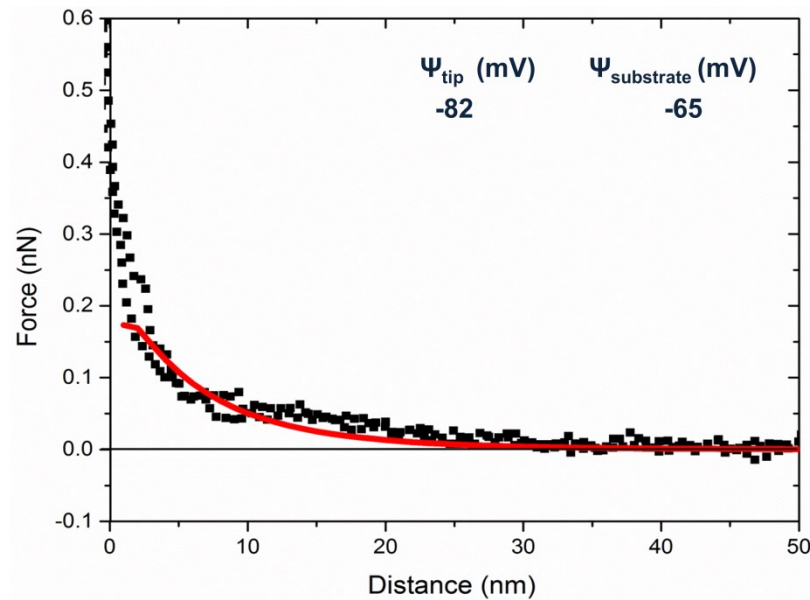
Figure 3-9 Typical force-distance profile measured between a silicon nitride tip and a silica wafer at pH 10.1 in 1 mM KCl solution. Symbols correspond to the experimental data. The solid curve represents the theoretical DLVO fitting based on constant surface charge density boundary condition.

3.3.3.2 Interactions between a silicon nitride tip and mineral surfaces

The interactions between a silicon nitride AFM tip with serpentine, olivine, and magnesite surfaces at pH 10.1 in 1 mM KCl solution were shown in Figure 3-10, 3-11, and 3-12, respectively. Approaching force profile between the silicon nitride tip and serpentine surface at pH 10.1 in 1 mM KCl solution is shown in Figure 3-10a. A representative image of serpentine surface is shown in Figure 3-10b. The imaging of the mineral surface allows for characterization of the surface prior to performing force measurements. Through obtaining an image, appropriate locations can be selected where surface force measurements can be performed. A smooth area with root-mean-square roughness (Rq) less than 1 nm is more desirable (Lin et al., 1993).

Figure 3-10b shows that although overall the serpentine surface was rough with a root-mean-square roughness of 19.26 nm over an area of 10×10 μm^2, smaller smooth regions with root-mean-square roughness of <1 nm could be easily located, as indicated by a dark square regime of 0.5×0.5 μm^2.

The Hamaker constant for serpentine-water-silicon nitride tip was calculated to be 2.17×10^{-20} J, based on the data given in Table 3-1. The force measurement indicated a surface potential of 12 mV on serpentine, as shown in Figure 3-10a. It should be noted that serpentine crystal structure consists of silica tetrahedral and brucite octahedral layers (Mookherjee and Stixrude, 2009). It is possible that the force measurement was performed on the brucite face of serpentine. Since the isoelectric point of brucite was reported around pH 11 (Pokrovsky and Schott, 2004), a surface potential of 12 mV is possible at pH 10.1. Similar observation

was also found for the silicon nitride tip and kaolinite system (Gupta and Miller, 2010).

Figure 3-10 The force measurement between a silicon nitride AFM tip and serpentine surface at pH 10.1 in 1 mM KCl solution: (a) typical force-distance profile, and (b) an AFM image of the prepared serpentine surface. Symbols correspond to the experimental data. The solid line represents the theoretical DLVO prediction using constant surface charge density boundary condition.

Approaching force-distance profile between the silicon nitride tip and olivine surface at pH 10.1 in 1 mM KCl solution is shown in Figure 3-11a. A representative topographic AFM image of olivine surface is shown in Figure 3-11b. The olivine surface had a root-mean-square roughness of 1.21 nm over an area of 10×10 μm^2. A local smooth region of root-mean-square roughness of 0.33 nm could be easily located as indicated by a dark square regime of 0.5×0.5 μm^2 shown in Figure 3-11b.

The measured force profiles and the DLVO model fitting are shown in Figure 3-11a. The Hamaker constant for olivine-water-silicon nitride tip was calculated to be 3.12×10^{-20} J, based on the data given in Table 3-1. Repulsive interaction

49

was observed between the silicon nitride tip and olivine surface during approach. The silicon nitride tip was observed to jump into contact with the olivine surface at ~5 nm which was attributed to the higher Hamaker constant (thus stronger van der Waals attraction) and lower electrical double layer repulsion as compared to the other two cases in Figures 3-9 and 3-10. The fitted surface potential of olivine surface was -65 mV in this study, as compared to the -25 mV from the zeta potential measurement. The difference may be due to the lower salt concentration of the solution used in the force measurement, as compared to the one used for zeta potential measurement.
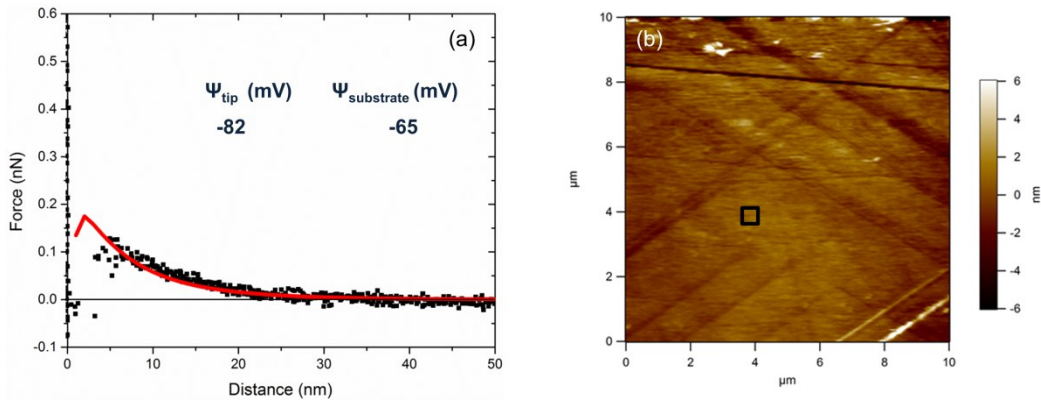
Figure 3-11 The force measurement between a silicon nitride AFM tip and olivine surface at pH 10.1 in 1 mM KCl solution: (a) typical force-distance profile, and (b) an AFM image of prepared olivine surface. Symbols correspond to the experimental data. The solid line represents the theoretical DLVO prediction using constant surface charge density boundary condition.

Approaching force-distance profile between the silicon nitride tip and magnesite surface at pH 10.1 in 1 mM KCl solution is shown in Figure 3-12a. A representative topographic image of magnesite surface is shown in Figure 3-12b.

The magnesite surface had a root-mean-square roughness of 1.48 nm over an area of 10×10 μm^2. A local smooth area of root-mean-square roughness of 0.34 nm could be easily located for force measurement as indicated by a dark square regime of 0.5×0.5 μm^2 shown in Figure 3-12b.

The interaction between the silicon nitride tip and magnesite surface on approach was found to be slightly attractive. The measured force-distance profiles and the DLVO model fitting are shown in Figure 3-12a. The Hamaker constant for magnesite-water-silicon nitride tip in water was calculated to be 3.37×10^{-20} Joule, based on the data given in Table 3-1. The fitted surface potential of magnesite surface was -7 mV in this study. Interestingly, it is quite similar to the zeta potential value obtained previously. The weak attraction measured was mainly attributed to the dominant attractive van der Waals interaction over the much weaker electrical double layer repulsion.
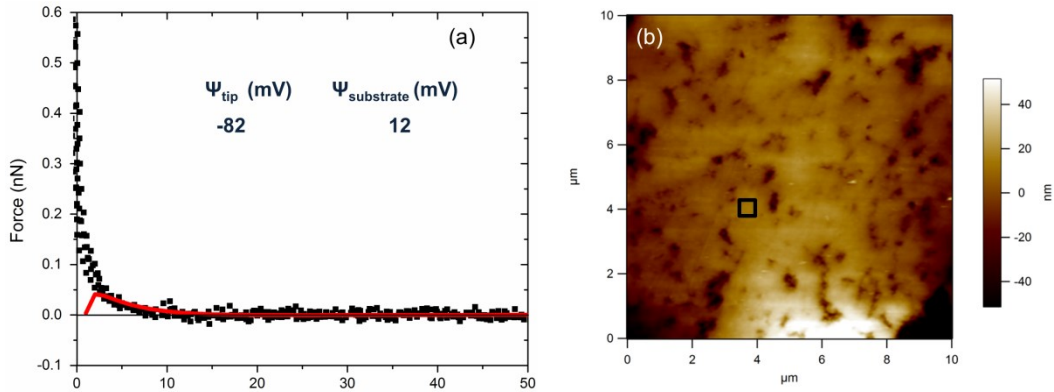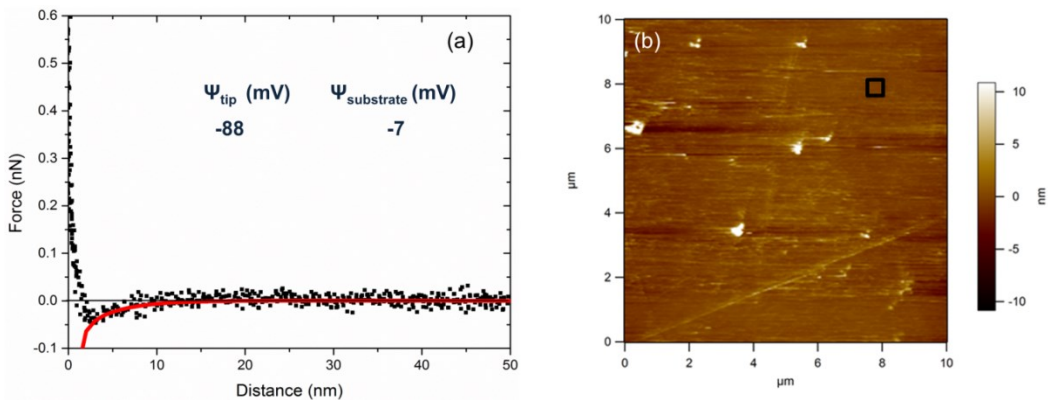

Figure 3-12 The force measurement between a silicon nitride AFM tip and magnesite surface at pH 10.1 in 1 mM KCl solution: (a) typical force-distance profile, and (b) an AFM image of prepared magnesite surface. Symbols

correspond to the experimental data. The solid line represents the theoretical

DLVO prediction using constant surface potential boundary condition.

3.3.4 Interaction mechanisms of different minerals

The zeta potential distribution and AFM force measurements provide valuable complementary information on the interaction mechanisms of different minerals. Figure 3-13 shows the schematic of proposed interaction mechanism between pentlandite and different gangue minerals (i.e., serpentine, olivine, and magnesite) at pH 10.1 in 10 mM KCl solution. Strong attraction is present in the pentlandite-serpentine system, as illustrated in Figure 3-13a. As discussed in previous section, serpentine is composed of silica tetrahedral and brucite octahedral layers. Our AFM force measurement also indicated a positively charged surface on serpentine, which may be from the brucite layer. It should also be noted that brucite has an isoelectric point at pH 11 (Pokrovsky and Schott, 2004). Therefore, it is expected that the brucite layer is positively charged at pH 10.1. In 10 mM KCl solution at pH 10.1, theoretically the silica layer of serpentine is negatively charged while the brucite layer is positively charged. It is very likely that the strong attraction observed in pentlandite-serpentine system is mainly due to the attraction between the brucite layer of serpentine and the pentlandite surface (Figure 3-13a). In pentlandite-olivine system strong repulsion exists between the two minerals (Figure 3-13b). The AFM force measurement shows a repulsive energy barrier when a negatively charged AFM tip approaches toward a negatively charged olivine surface. In the colloidal system of pentlandite and olivine, this energy barrier prevents a hetero coagulation between a negatively

charged pentlandite and a negatively charged olivine. In pentlandite-magnesite system, a weaker repulsion between the two minerals may be present (Figure 3-13c). As opposed to the strong repulsion observed in pentlandite-olivine system, the weak repulsion observed in pentlandite-magnesite system is mainly due to the smaller magnitude of magnesite's surface potential.
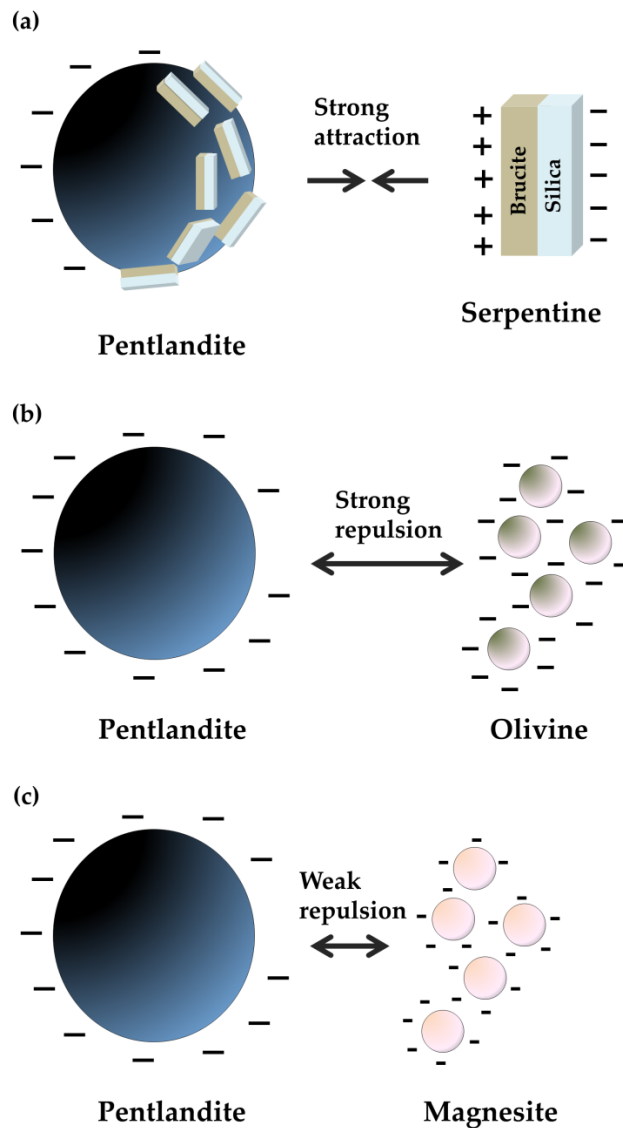
Figure 3-13 Schematic for binary particulate component systems which can be interpreted for particle interactions in: (a) pentlandite-serpentine, (b) pentlandite-

olivine, and (c) pentlandite-magnesite systems. The interactions were based on the zeta potential distribution measurements taken at pH 10.1 in 10 mM KCl solution.

In terms of the flotation at pH 10.1, the presence of different gangue minerals may impose different effects toward pentlandite recovery. The presence of serpentine induces slime coating, which results in poor pentlandite recovery (Bremmel et al., 2005; Edwards et al., 1980). However, slime coating is not expected in the presence of olivine or magnesite. Repulsion between pentlandite and olivine or magnesite occurs due to the negative surface charge of the minerals. Other report has shown that the presence of the negatively charged quartz does not significantly affect the flotation of pentlandite (Feng et al., 2012a). Therefore it is predicted that the presence of olivine or magnesite will not be detrimental on the pentlandite recovery.

3.4 Conclusions

In this study, the interaction mechanisms of pentlandite and gangue minerals were investigated using zeta potential distribution measurements. In addition, AFM was employed to study the interaction between different mineral surfaces with a negatively charged AFM silicon nitride tip (which represents a negatively charged pentlandite). The pentlandite and serpentine have strong attractive interaction, as observed in the zeta potential distribution measurements, which suggests a slime coating of serpentine on pentlandite surface. Repulsive interaction is also present in the pentlandite-olivine and pentlandite-magnesite systems, as evident from the zeta potential distribution measurements. AFM force measurement indicated a

positive surface potential on serpentine surface. This is possibly due to the measurement being taken on the brucite face of serpentine. Repulsive interaction was observed in the AFM force measurement between the silicon nitride tip and olivine surface during approach. At separation distance ~5 nm, the silicon nitride tip was observed to jump into contact with the olivine surface which was due to stronger van der Waals attraction and lower electrical double layer repulsion. The measured surface potential of olivine is higher than the one obtained from zeta potential measurement. This is very likely due to the lower salt concentration used in the force measurement. AFM force measurement shows attractive interaction between the silicon nitride tip and magnesite surface on approach, which is mainly due to the dominant van der Waals attraction over the much weaker electrical double layer repulsion. The measured surface potential on magnesite surface agrees with the zeta potential measurement.

In the flotation, the presence of serpentine will have detrimental effect on pentlandite recovery due to slime coating. The presence of olivine and magnesite, however, may not depress pentlandite recovery, which was mainly due to the repulsive interaction between pentlandite and olivine or magnesite.

3.5 References

Alvarez-Silva, M. (2011) *Surface chemistry study on the pentlandite-serpentine system, PhD Dissertation*, McGill University.

Alvarez-Silva, M., Mirnezami, M., Uribe-Salas, A., Finch, J.A. (2010) 'Point of zero charge, isoelectric point and aggregation of phyllosilicate minerals', *Canadian Metallurgical Quarterly*, vol. 49, no. 4, pp. 405–410.

Baas-Becking, L.G., Galliher, E.W. (1931) 'Wall structure and mineralization in coralline algae', *The Journal of Physical Chemistry*, vol. 35, no. 2, pp. 467-479.

Bergström, L. (1997) 'Hamaker constants of inorganic materials', *Advances in Colloid and Interface Science*, vol. 70, pp. 125-169.

Bobicki, E.R., Liu, Q., Xu, Z. (2014) 'Microwave heating of ultramafic nickel ores and mineralogical effects', *Minerals Engineering*, vol. 58, pp. 22-25.

Bremmel, K.E., Fornasiero, D., Ralston, J. (2005) 'Pentlandite-lizardite interactions and implications for their separation by flotation', *Colloids and Surfaces A: Physicochemical and Engineering Aspects*, vol. 252, pp. 207–212.

Brindley, G. W., Hayami, R. (1964) 'Kinetics and mechanisms of dehydration and recrystallization of serpentine: I', *Clays and Clay Minerals*, vol. 12, pp. 35-47.

Cattaneo, A., Gualtieri, A. F., Artioli, G. (2003) 'Kinetic study of the dehydroxylation of chrysotile asbestos with temperature by in situ XRPD', *Physics and Chemistry of Minerals*, vol. 30, no. 3, pp. 177-183.

Dai, Z., Bos, J.A., Quinn, P., Lee, A., Xu, M. (2009) 'Flowsheet development for Thompson ultramafic low-grade nickel ores', *Proceedings of the 48th annual conference of metallurgists of CIM*, Met Soc, Sudbury, Ontario, Canada, pp. 217–228.

Drelich, J., Long, J., Yeung, A. (2007) 'Determining surface potential of the bitumen-water interface at nanoscale resolution using atomic force microscopy', *The Canadian Journal of Chemical Engineering*, vol. 85, no. 5, pp. 625–634.

Edwards, C.R., Kipkie, W.B., Agar, G.E. (1980) 'The effect of slime coatings of the serpentine minerals, chrysotile and lizardite, on pentlandite flotation', *International Journal of Mineral Processing*, vol. 7, pp. 33–42.

Feng, B., Feng, Q., Lu, Y. (2012a) 'A novel method to limit the detrimental effect of serpentine on the flotation of pentlandite', *International Journal of Mineral Processing*, vol. 114-117, pp. 11–13.

Feng, B., Lu, Y., Feng, Q., Zhang, M., Gu, Y. (2012b) 'Talc-serpentine interactions and implications for talc depression', *Minerals Engineering*, vol. 32, pp. 68–73.

Feng, B., Lu, Y., Feng, Q., Ding, P., Luo, N. (2013) 'Mechanisms of surface charge development of serpentine mineral', *Transactions of Nonferrous Metals Society of China*, vol. 23, no. 4, pp. 1123–1128.

Game, P.M. (1941) 'Optical properties of olivines from Ubekendt Island, West Greenland', *Mineralogical Magazine*, vol. 26, no. 172, pp. 11–15.

Gualtieri, A.F., Gemmi, M., Dapiaggi, M. (2003) 'Phase transformations and reaction kinetics during the temperature-induced oxidation of natural olivine', *American Mineralogist*, vol. 88, pp. 1560–1574.

Gualtieri, A.F., Giacobbe, C., Viti, C. (2012) 'The dehydroxylation of serpentine group minerals', *American Mineralogist*, vol. 97, pp. 666–680.

Gupta, V., Miller, J.D. (2010) 'Surface force measurements at the basal planes of ordered kaolinite particles', *Journal of Colloid and Interface Science*, vol. 344, pp. 362–371.

Huang, Z., Li, W., Pan, Z., Liu, Y., Fang, M. (2013) 'High-temperature transformation of asbestos tailings by carbothermal reduction', *Clays and Clay Minerals*, vol. 61, no. 1, pp. 75-82.

Israelachvili, J. (2011) *Intermolecular and surface forces*, 3rd ed., Academic Press, London.

Leonelli, C., Veronesi, P., Boccaccini, D.N., Rivasi, M.R., Barbieri, L., Andreola, F., Lancellotti, I., Rabitti, D., Pellacani, G.C. (2006) 'Microwave thermal inertisation of asbestos containing waste and its recycling in traditional ceramics', *Journal of Hazardous Materials B*, vol. 135, pp. 149-155.

Lin, X.Y., Creuzet, F., Arribart, H. (1993) 'Atomic force microscopy for local characterization of surface acid-base properties', *Journal of Physical Chemistry*, vol. 97, pp. 7272–7276.

Liu, J., Zhou, Z., Xu, Z., Masliyah, J. (2002) 'Bitumen-clay interactions in aqueous media studied by zeta potential distribution measurement', *Journal of Colloid and Interface Science*, vol. 252, pp. 409–418.

Liu, J., Xu, Z., Masliyah, J. (2003) 'Studies on bitumen-silica interaction in aqueous solutions by atomic force microscopy', *Langmuir*, vol. 19, pp. 3911–3920.

Liu, J., Xu, Z., Masliyah, J. (2004a) 'Interaction between bitumen and fines in oil sands extraction system: implication to bitumen recovery', *The Canadian Journal of Chemical Engineering*, vol. 82, no. 4, pp. 655–666.

Liu, J., Xu, Z., Masliyah, J. (2004b) 'Role of fine clays in bitumen extraction from oil sands', *AIChE Journal*, vol. 50, no. 8, pp. 1917–1927.

Liu, J., Xu, Z., Masliyah, J. (2005) 'Interaction forces in bitumen extraction from oil sands', *Journal of Colloid and Interface Science*, vol. 287, no. 2, pp. 507–520.

Masliyah, J., Czarnecki, J., Xu, Z. (2011) *Handbook on theory and practice of bitumen recovery from Athabasca oil sands*, Kingsley, Canada.

Merve Genc, A., Kilickaplan, I., Laskowski, J.S. (2012) 'Effect of pulp rheology on flotation of nickel sulphide ore with fibrous gangue particles', *Canadian Metallurgical Quarterly*, vol. 51, no. 4, pp. 368–375.

Minowa, T., Yoshikawa, M., Honshima, M. (1989) 'Improvement of the corrosion resistance on Nd-Fe-B magnet with nickel plating', *IEEE Transactions on Magnetics*, vol. 25, no. 5, pp. 3776–3778.

Mookherjee, M., Stixrude, L. (2009) 'Structure and elasticity of serpentine at high-pressure', *Earth and Planetary Science Letters*, vol. 279, pp. 11–19.

Mooney, T., Knacke, R.F. (1985) 'Optical constants of chlorite and serpentine between 2.5 and 50 μm', *Icarus*, vol. 64, pp. 493–502.

Parks, G.A. (1965) 'The isoelectric points of solid oxides, solid hydroxides, and aqueous hydroxo complex systems', *Chemical Reviews*, vol. 65, no. 2, pp. 177-198.

Parks, G.A. (1967) 'Aqueous surface chemistry of oxides and complex minerals', In *Equilibrium Concepts in Natural Water Systems*, pp. 121-160, American Chemical Society.

Pokrovsky, O.S., Schott, J. (2004) 'Experimental study of brucite dissolution and precipitation in aqueous solutions: Surface speciation and chemical affinity control', *Geochimica et Cosmochimica Acta*, vol. 68, no. 1, pp. 31–45.

Rahilly, G., Price, N. (2003) 'Current products and practice Nickel allergy and orthodontics', *Journal of Orthodontics*, vol. 30, pp. 171–174.

Rosenholtz, J.L., Smith, D.T. (1936) *The dielectric constant of mineral powders*, Rensselaer Polytechnic Institute.

Viti, C. (2010) 'Serpentine minerals discrimination by thermal analysis', *American Mineralogist*, vol. 95, no. 4, pp. 631-638.

Xu, Z., Liu, J., Choung, J.W., Zhou, Z. (2003) 'Electrokinetic study of clay interactions with coal in flotation', *International Journal of Mineral Processing*, vol. 68, pp. 183-196.

Xu, M., Dai, Z., Dong, J., Ford, F., Lee, A. (2010) 'Fibrous minerals in ultramafic nickel sulphide ores', *Proceedings of the 49th annual conference of metallurgists*, Met Soc, Vancouver, British Columbia, Canada, pp. 223–235.

Yan, L., Masliyah, J.H., Xu, Z. (2013) 'Understanding suspension rheology of anisotropically-charged platy minerals from direct interaction force measurement using AFM', *Current Opinion in Colloid & Interface Science*, vol. 18, pp. 149-156.

Yan, L., Englert, A.H., Masliyah, J.H., Xu, Z. (2011) 'Determination of anisotropic surface characteristics of different phyllosilicates by direct force measurements', *Langmuir*, vol. 27, pp. 12996–13007.

Yin, X., Drelich, J. (2008) 'Surface charge microscopy: novel technique for mapping charge-mosaic surfaces in electrolyte solutions', *Langmuir*, vol. 24, pp. 8013–8020.

Zhang, Q., Wu, M., Zhao, W. (2005) 'Electroless nickel plating on hollow glass microspheres', *Surface and Coatings Technology*, vol. 192, pp. 213–219.

Zhao, H., Bhattacharjee, S., Chow, R., Wallace, D., Masliyah, J., Xu, Z. (2008) 'Probing surface charge potentials of clay basal planes and edges by direct force measurements', *Langmuir*, vol. 24, pp. 12899–12910.

Zussman, J. (1978) 'The crystal structures of amphibole and serpentine minerals',

Proceedings of the workshop on asbestos, definitions and measurement

method, The Bureau, Maryland, pp. 35–48.

Chapter 4 Effect of the Presence of Fine Minerals Particles towards Pentlandite Flotation[2]

4.1 Introduction

Nickel has been widely used in plating, in production of stainless steel, as well as in other corrosion and wear resistant materials (Minowa et al., 1989; Rahilly and Price, 2003; Zhang et al., 2005). Due to the declining number of high-grade nickel ores, the low-grade ultramafic nickel ores are becoming important alternative sources of nickel (Dai et al., 2009; Merve Genc et al., 2012). A common gangue mineral, such as serpentine, is mostly encountered in this ultramafic nickel and leads to a significant difficulty during the flotation (Bremmel et al., 2005; Merve Genc et al., 2012; Pietrobon et al., 1997; Senior and Thomas, 2005; Wellham et al., 1992).

Problems such as high pulp viscosity and slime coating on the valuable nickel bearing mineral (i.e. pentlandite) significantly reduce the nickel recovery and grade concentrate during flotation (Merve Genc et al., 2012; Wellham et al., 1992). The high pulp viscosity is mainly attributed to the presence of serpentine in the low-grade ultramafic nickel ore (Dai et al., 2009). The presence of fibrous minerals is also responsible for the formation of air bubble-macro fibres aggregates, leading to the recovery of MgO-containing minerals (Xu et al., 2010).

The interaction between pentlandite and serpentine has been studied previously (Bremmel et al., 2005; Edwards et al., 1980) and this interaction leads to the slime

---

[2] A version of this chapter will be submitted for publication on *Minerals Engineering* journal.

coating on pentlandite surface. The formation of slime coating is mainly attributed to the attractive interaction between a negatively charged pentlandite and a positively charged serpentine. Slime coating leads to the loss of nickel recovery, since pentlandite becomes hydrophilic after the coating of serpentine (Alvarez-Silva, 2011). The presence of serpentine in the nickel concentrate results in the higher smelting cost due to higher slag melting point (Alvarez-Silva, 2011; Beattie et al., 2006; Feng et al., 2013).

The MgO-containing minerals in the low-grade nickel ores mainly include serpentine and olivine. Serpentine has a layered structure which is comprised of 1:1 layering of one silica (SiO_4) tetrahedral layer bonded to a brucite (Mg-O) octahedral layer, which are held together by van der Waals forces (Alvarez-Silva et al., 2010a; 2010b; Mookherjee and Stixrude, 2009). Some common polymorphs of serpentine are: chrysotile, antigorite, and lizardite. Chrysotile is a fibrous, tubular mineral and classified as asbestos (Zussman, 1978). On the contrary, antigorite has a curved, corrugated sheet structure while lizardite has a flat-layered and platy structure (Zussman, 1978). As opposed to serpentine, olivine is an orthosilicate mineral consisting of isolated SiO_4 tetrahedral connected via divalent cations (i.e. magnesium and iron) in six fold coordination and it has no layered structure (Gualtieri et al., 2003).

Thermal pretreatment of the ultramafic nickel ores has been investigated as a way to improve flotation by reducing or eliminating the negative effects of serpentine (Bobicki et al., 2014). It is known that serpentine transforms into olivine at above the dehydroxylation temperature (Gualtieri et al., 2012; Huang et al., 2013;

64

Leonelli et al., 2006).In another aspect of flotation, sodium carbonate is also widely used in nickel ore processing to control the precipitation of magnesium hydroxide by sequestering magnesium to form magnesite (Alvarez-Silva, 2011). It is important to understand the effect of serpentine, olivine, and magnesite fines on the flotation of pentlandite. To accomplish this, basic and fundamental studies such as contact angle and induction time measurements were performed to determine the hydrophobicity of the minerals. Furthermore, a small scale flotation tests were performed to obtain clearer evidence in this study. The non-floating components from the flotation of pentlandite in presence of fine minerals were characterized by the scanning electron microscope with the energy dispersive X-ray spectra (SEM-EDX). This study provides new insights into the interaction between pentlandite with other minerals in the flotation of low-grade nickel sulphide ore.

4.2 Experimental

4.2.1 Materials and reagents

Serpentine and olivine rocks were obtained from Ward's Natural Science Establishment, while magnesite rock was obtained from Minerals Unlimited, USA. Magnesium carbonate powder was obtained from Fisher Scientific and used as supplied in the flotation study. High purity pentlandite sample was obtained from Vale Base Metals Technology Development (Mississauga, Ontario, Canada). Serpentine and olivine were crushed and sieved to obtain -38 μm size fractions. Pentlandite sample was sieved to obtain +45 /-75 μm size fractions.

Some of the serpentine, olivine, and magnesite rocks were kept for contact angle and induction time measurements. Pentlandite was washed using 0.1 M hydrochloric acid and acetone to remove the oxidation layer and chemical residue.

For the contact angle and induction time measurements, the rock pieces of serpentine, olivine, and magnesite minerals were mounted in an epoxy resin (West System Inc., Bay City, MI, USA) and cured into reaching solid state. The samples were polished to expose and flatten the mineral surface. A wet grinding using 45 μm grinding paper was performed, followed by series of polishing using diamond slurry (9 μm and 3 μm) and alumina slurry (0.05 μm). The samples were then washed and sonicated in Milli-Q water to remove the polishing suspensions. For the purpose of contact angle measurement, the pentlandite powder was pressed to form a pellet.

Hydrochloric acid (HCl) and potassium hydroxide (KOH) from Fisher Scientific were used as pH modifiers in this study. Potassium chloride (KCl) from Fisher Scientific was used for preparing the supporting electrolyte solution. Potassium amyl xanthate (PAX) was supplied by Prospec Chemicals Ltd. (Canada) and purified by using the method as described by Rao (1971). Deionized water (Milli-Q water) with a resistivity of 18.2 MΩ cm prepared with Millipore Elix 5 purification system was used in this study.

4.2.2 Contact angle measurements

Contact angle measurement was performed to obtain a measure of hydrophobicity of different minerals. To do the measurements, the pentlandite powder was

pressed to form a pellet; the rock pieces of serpentine, olivine, and magnesite minerals were mounted in an epoxy resin (West System Inc., Bay City, MI, USA). The samples were polished to obtain flat mineral surface. A wet grinding using 45 μm grinding paper was performed, followed by series of polishing using diamond slurry (9 μm and 3 μm) and alumina slurry (0.05 μm). The samples were then washed and sonicated in Milli-Q water to remove the slurry suspension residue.

A goniometer (Ramé-Hart Instrument, USA) was used to measure the contact angle of a liquid droplet on the mineral surface. A 10 mM KCl solution at pH 10.1 was used in this contact angle measurement. The pH 10.1 was selected based on the operation practice at the Thompson Mill (Dai et al., 2009). The contact angle was measured at least on nine different locations on the mineral surface.

4.2.3 Induction time measurements

The induction time setup used in this study was based on a version used by Gu et al. (2003). A 10 mM KCl solution was used as the supporting electrolyte. The samples (serpentine, olivine, and magnesite) prepared for the contact angle measurements were used for the induction time measurements. For the induction time measurements of pentlandite, the pentlandite particle bed was prepared on a silica wafer plate. A minimum of 20 measurements on every pre-set contact time was taken. The induction time was defined as the time at which 50% of the observations resulted in attachment of air bubble on the particle or substrate (Ye and Miller, 1988).

Figure 4-1 shows the "attachment" or "no attachment" case of air bubble in contact with substrate or a particle bed after a period of time. During the full contact with the substrate or particle bed, the air bubble is at a deformed state (Figure 4-1, left). During the retraction, an "attachment" case can be judged by an attaching air bubble on the substrate or by the attachment of particles on air bubble (Figure 4-1, upper-right). Consequently, the "no attachment" case can be judged by the non-attachment of the substrate or particles on air bubble during retraction (Figure 4-1, lower-right).
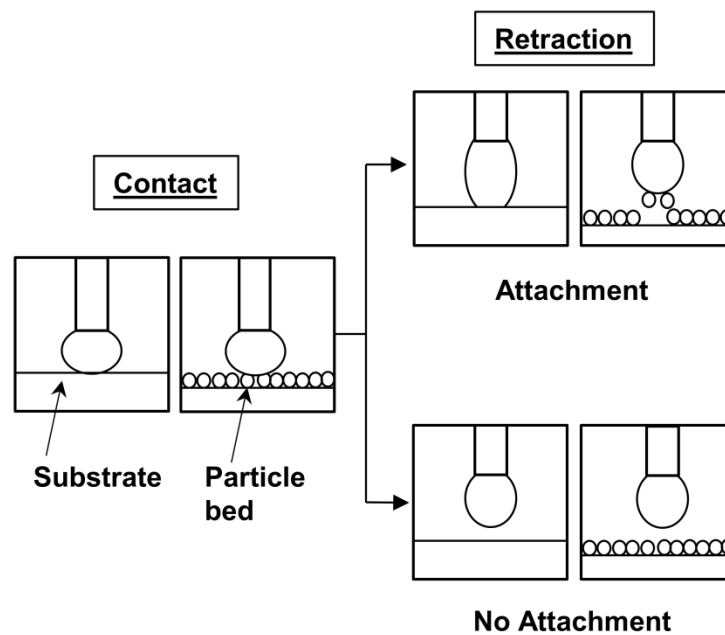
Figure 4-1 Schematic of the "attachment" or "no attachment" case after air bubble is in contact with a substrate or a particle bed.

4.2.4 Small scale flotation tests

The flotation tests were carried out in a modified Hallimond tube. A high purity N_2 gas was used to generate bubbles and set at a flow rate of 30 sccm (Standard

68

Cubic Centimetres per Minute). About 1.5 gr of pentlandite (+45 /-75 µm size fractions) were used in each test. A 1 mM KCl solution was used as the supporting electrolyte. The pH of the pentlandite slurry was adjusted, and the slurry was then conditioned with PAX for five minutes. The flotation was run for five minutes, and the concentrate was collected every one minute. In the case of the flotation with the presence of fine minerals, the fine minerals (-38 µm size fractions) were added together with pentlandite into the supporting electrolyte prior to pH adjustment and PAX conditioning. The fine minerals concentration levels were set to 4% and 1.3% (with respect to the mass of pentlandite). The non-floating components from the flotation of pentlandite in presence of fine minerals were characterized by the scanning electron microscope with the energy dispersive X-ray spectra (SEM-EDX, Hitachi S-2700).

4.3 Results and discussion

4.3.1 Contact angle measurements on different minerals

The surface hydrophobicity of the gangue minerals (i.e. serpentine, olivine, magnesite) and the valuable mineral (i.e. pentlandite) was investigated by contact angle measurements. Contact angle is one of an important parameter in mineral flotation (Chau et al., 2009). The measured contact angle values at different mineral surfaces are shown in Figure 4-2 and summarized in Table 4-1.
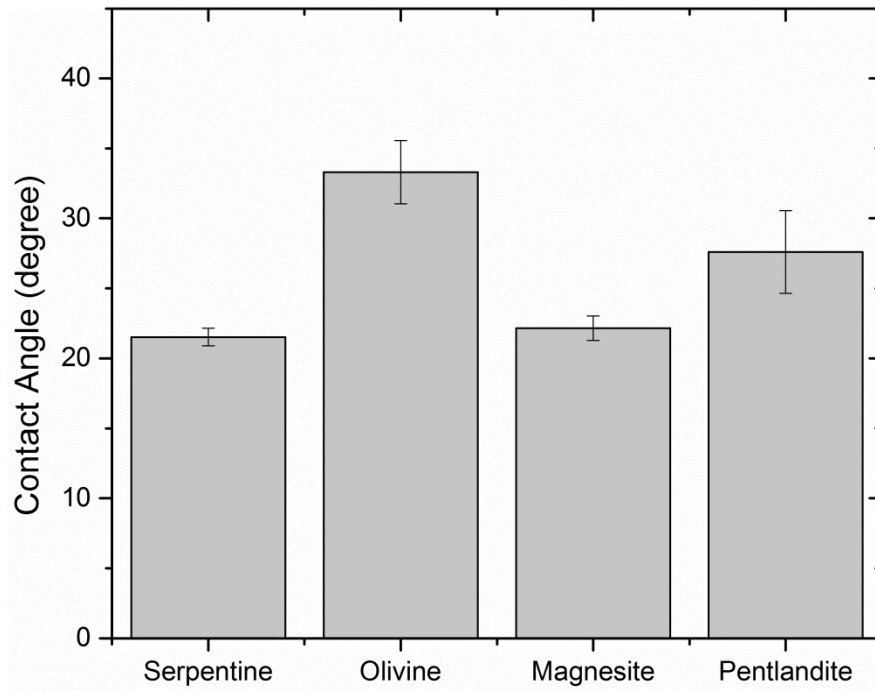
Figure 4-2 The contact angles of different minerals at pH 10.1 in 10 mM KCl
solution.

Table 4-1 The contact angle values of different minerals.

Materials	Contact angle
Serpentine	$21.5 \pm 0.6^{\circ}$
Olivine	$33.3 \pm 2.3^{\circ}$
Magnesite	$22.2 \pm 0.9^{\circ}$
Pentlandite	$27.6 \pm 2.9^{\circ}$

From the contact angle measurements, olivine showed the highest degree of
hydrophobicity among the gangue minerals, with a contact angle of $33.3 \pm 2.3^{\circ}$.
Pentlandite also showed a comparable degree of hydrophobicity as olivine, with a
contact angle of $27.6 \pm 2.9^{\circ}$. Serpentine had a quite similar contact angle with

magnesite, 21.5±0.6 $^{\circ}$ and 22.2±0.9 $^{\circ}$ for serpentine and magnesite, respectively. Lu et al. (2009) reported a contact angle of 37.6 $^{\circ}$ for serpentine. Gence (2006) reported a contact angle of about 11.5 $^{\circ}$ for magnesite at pH 10. Alvarez-Silva (2011) reported a value of close to 0 $^{\circ}$ for pentlandite contact angle at pH 10 without the presence of PAX. No contact angle value has been reported for olivine. The different contact angle values reported here and in literature may be due to difference in samples, solution condition, and experimental technique.

It should be noted that the contact angle measurements on the gangue minerals were different than the measurements taken for the pentlandite. The contact angle measurements for the gangue minerals were performed on a flat, polished mineral substrate; while the measurements for pentlandite were performed on a flat, powder pellet of pentlandite. Hence, the roughness factor was more significant for the pentlandite contact angle measurements, since surface roughness contributes to the difficulty of assigning the true apparent contact angle (Chau et al., 2009).

4.3.2 Induction time measurements on different minerals

The measurements of induction time provide important parameter about air bubble-mineral attachment in flotation. The attachment process involves the thinning and rupture of the wetting film between the air bubble and mineral surface (Su et al., 2006). Induction time measurements was used to investigate the surface hydrophobicity of the gangue minerals (i.e. serpentine, olivine, magnesite) and the valuable mineral (i.e. pentlandite), in addition to the contact angle measurements. The induction time measurement of air bubble attaching to

serpentine, olivine, magnesite, and pentlandite at pH 10.1 in 10 mM KCl solution is shown in Figure 4-3.

Figure 4-3 shows the attachment frequency distribution as a function of contact time between the air bubble and different minerals surfaces (i.e., serpentine, olivine, magnesite, and pentlandite) at pH 10.1 in 10 mM KCl solution. The induction time was calculated to be 180.6, 161.5, 256.0, 27.1 ms for serpentine, olivine, magnesite, and pentlandite, respectively, by using Boltzmann curve fitting. The results are summarized in Table 4-2.
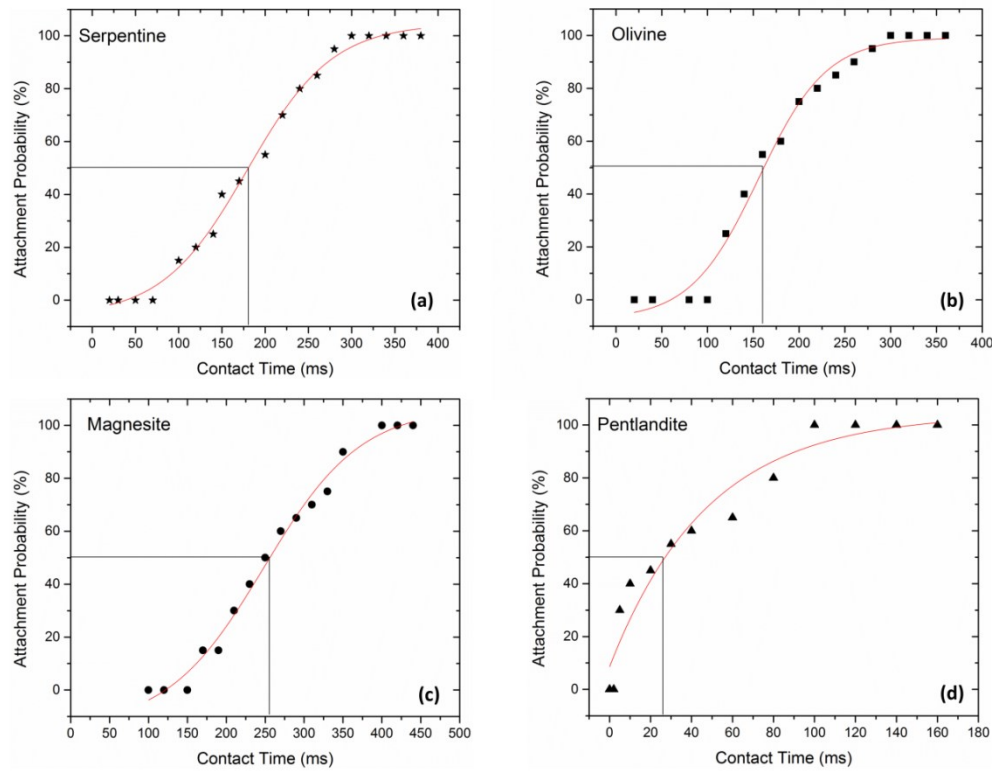
Figure 4-3 Induction time measurement of air bubbles attaching to different mineral surfaces at pH 10.1 in 10 mM KCl solution. Induction time measurements for serpentine, olivine, and magnesite samples were performed on polished rock

on a resin, while measurement for pentlandite was performed on a pentlandite

particles bed.

It is well established that the shorter the induction time, the greater is the contact

angle (Ye and Miller, 1988). Therefore it implies that a shorter induction time

indicates a higher degree of hydrophobicity. Among the gangue minerals, olivine

had the shortest induction time (161.5 ms), followed by serpentine (180.6 ms) and

magnesite (256.0 ms). Based on the induction time measurements, olivine was the

most hydrophobic among the gangue minerals. These results are consistent with

the contact angle measurements, where olivine had higher contact angle (33.3 ^{o})

than both serpentine (21.5 ^{o}) and magnesite (22.2 ^{o}). Pentlandite, however, showed

a very short induction time (27.1 ms) as compared to the gangue minerals, which

indicated that pentlandite was indeed more hydrophobic than the gangue minerals.

Table 4-2 The air bubble induction time on different mineral surfaces.

Materials	Induction time (ms)
Serpentine	180.6
Olivine	161.5
Magnesite	256.0
Pentlandite	27.1

4.3.3 Flotation tests using a modified Hallimond tube

The small scale flotation tests were performed in order to study the effect of fines

on pentlandite recovery. Prior to performing flotation tests in the presence of fine

minerals, it is important to determine the optimum concentration of the collector

(PAX). Figure 4-4 shows the effect of PAX concentration on the pentlandite recovery in single mineral flotation tests (■ − recovery at pH 10.1, ▲ − recovery at pH 2.5). At pH 10.1, the recovery of pentlandite using 10^{-5} M PAX was very low at 16.2%. Increasing the PAX concentration to 3 x 10^{-4} increased the pentlandite recovery to 68.6% at pH 10.1. At pH 10.1 and by using 5 x 10^{-4} and 7 x 10^{-4} M PAX, the pentlandite recovery was significantly increased to 89.7% and 96.5%, respectively. For the purpose of this study, the PAX concentration of 5 x 10^{-4} M was selected. At pH 2.5 and by using 5 x 10^{-4} M PAX, the pentlandite recovery was found to be higher, which was 97.3%. The higher recovery at lower pH has been observed previously (Dai et al., 2009).
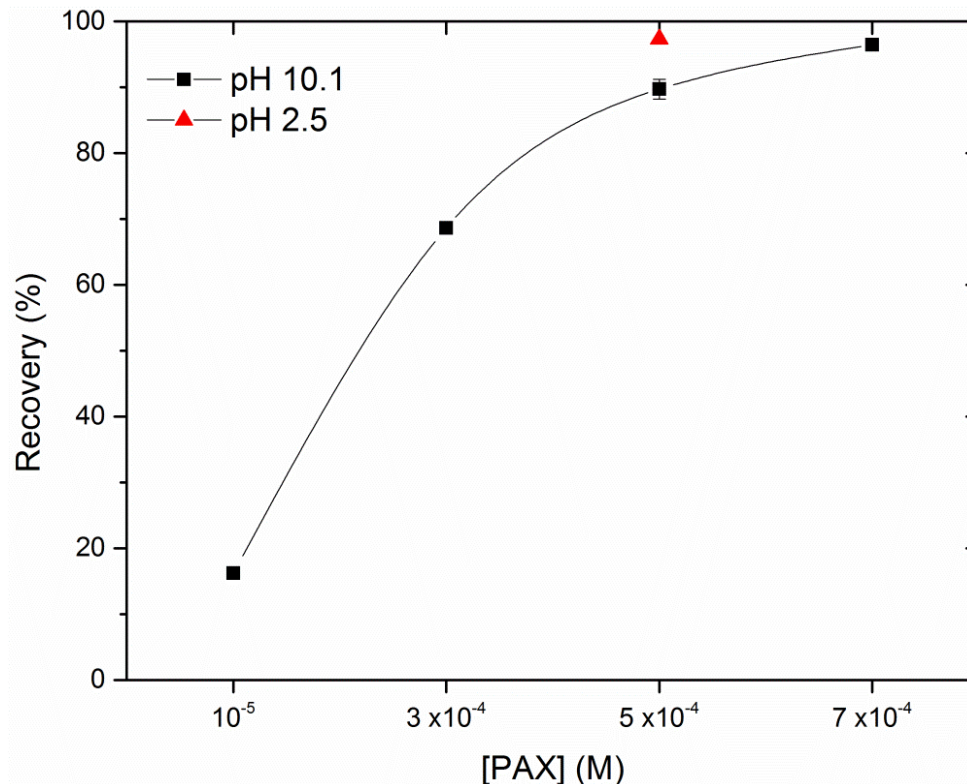
Figure 4-4 Effect of PAX concentration on the recovery of pentlandite in single mineral flotation tests (■ − recovery at pH 10.1, ▲ − recovery at pH 2.5).

The effect of serpentine (Sp) fines on pentlandite (Pn) recovery at pH 10.1 and pH 2.5 are shown in Figure 4-5a and 4-5b, respectively. At pH 10.1, the pentlandite recovery at Sp concentration of 1.3% and 4% were 73.8% (Figure 4-5a, ■) and 46.6% (Figure 4-5a, ▲), respectively. It is clear that the presence of serpentine diminished pentlandite recovery and the effect was more significant when serpentine concentration was increased. These results are comparable to the results obtained by Edwards et al. (1980). At pH 2.5, the pentlandite recovery at Sp concentration of 1.3% and 4% were 78.8% (Figure 4-5b, ■) and 54.3% (Figure 4-5b, ▲), respectively. At this pH, the presence of serpentine had less severe impact towards pentlandite recovery than at pH 10.1. Overall, the final pentlandite recovery was slightly higher at pH 2.5 than at pH 10.1 in the presence of serpentine. However, by comparing the initial flotation rate, the flotation rate at higher pH was slightly higher than at lower pH.
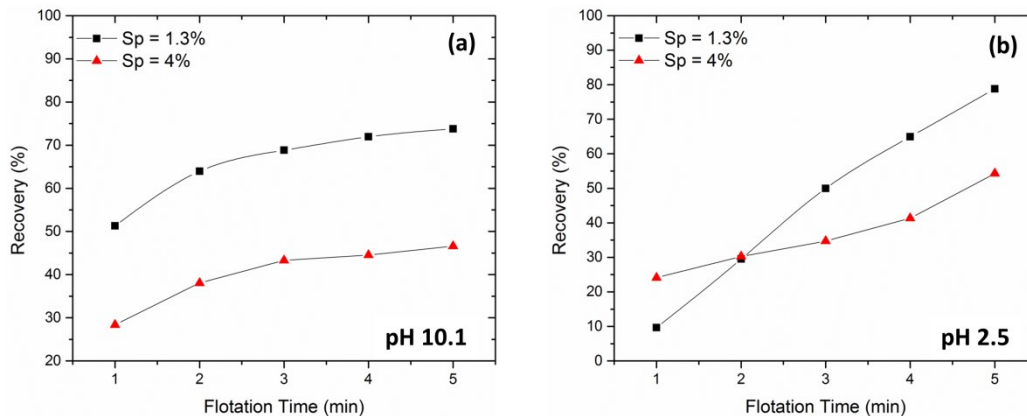
Figure 4-5 Recovery of pentlandite as a function of time and serpentine fines concentration (a) at pH 10.1, and (b) at pH 2.5 in 1 mM KCl and 5×10^{-4} M PAX solution (■ – Sp = 1.3%), ▲ – Sp = 4%).

Figure 4-6 shows the evidence of the attachment of serpentine particles on the pentlandite surface in the images of the non-floating pentlandite particles at pH 10.1 in 1 mM KCl solution, taken by using a scanning electron microscope (SEM) (Hitachi S-2700). The SEM images show the presence of fine serpentine particles and fibres (chrysotile).
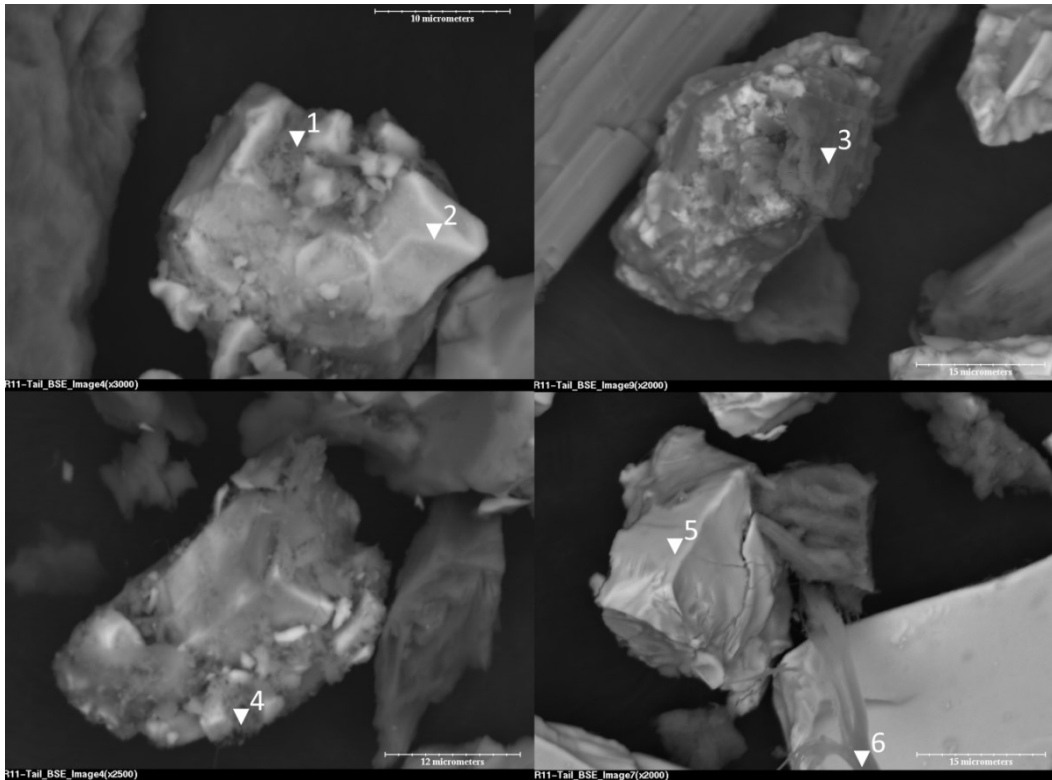
Figure 4-6 SEM images of the non-floating pentlandite particles coated with magnesium silicate particles and fibres at pH 10.1 in 1 mM KCl solution.

The energy dispersive X-ray (EDX) spectra taken at various locations of the non-floating pentlandite particles at pH 10.1 in 1 mM KCl solution are shown in Figure 4-7a to 4-7f. Figure 4-7b and 4-7e are the spectra taken at point 2 and point 5 (from Figure 4-6) that consist mainly of Fe, Ni, and S, which are expected for pentlandite. In Figure 4-7a, 4-7c, 4-7d, and 4-7f, the presence of Mg, Al, and Si

can be observed, which correlate to the presence of serpentine. This confirms the adsorption of serpentine slime particles and fibres onto pentlandite surface during flotation at pH 10.1. Similar observations have been observed previously (Bremmel et al., 2005; Edwards et al., 1980).
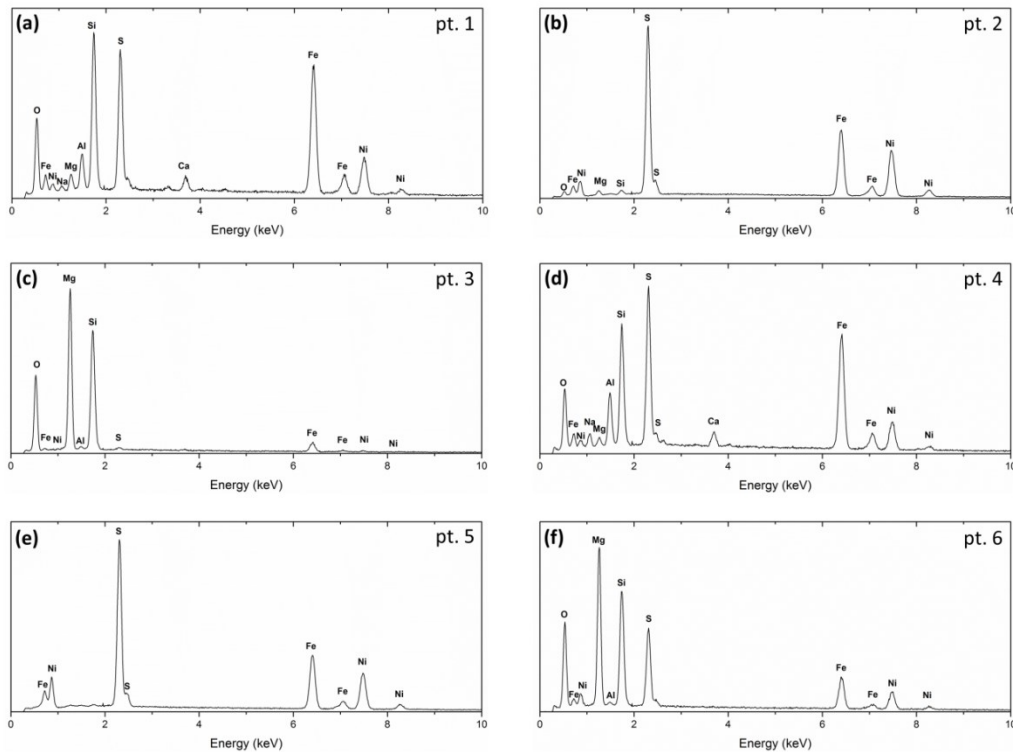
Figure 4-7 EDX spectra of the non-floating component from the pentlandite-serpentine flotation at pH 10.1 in 1 mM KCl solution. The spectra correspond to the points as indicated in Figure 4-6.

Figure 4-8 shows the X-Ray map of the non-floating component from the pentlandite-serpentine flotation at pH 2.5. The map shows a very small amount of serpentine, which is indicated by the presence of Mg, Al, and Si elements. Serpentine may get collected into the concentrate during flotation due to the lack

of flotation selectivity between pentlandite and silicate gangue minerals at pH lower than 10.1 (Dai et al., 2009).

Figure 4-8 X-Ray mapping of the non-floating component from the pentlandite-serpentine flotation at pH 2.5 in 1 mM KCl solution.

The SEM image and EDX spectrum of the pentlandite partially coated with magnesium silicate slime particles at pH 2.5 are shown in Figure 4-9a and 4-9b, respectively. The EDX spectrum indicates the presence of Mg, Al, and Si, which can be ascribed to the presence of serpentine. At pH 2.5, slime coating of serpentine on pentlandite surface may occur. At this pH, pentlandite is positively charged (Bremmel et al., 2005) while the silica face of serpentine is negatively charged (Miller et al., 2007; Parks, 1965; 1967). Other observation is also found

in a kaolinite system, where the silica face of kaolinite is negatively charged below pH 4 (Gupta and Miller, 2010). Therefore, it is possible that the slime coating mechanism is through the attractive electrostatic interaction between the positively charged pentlandite and the negatively charged silica face of serpentine.
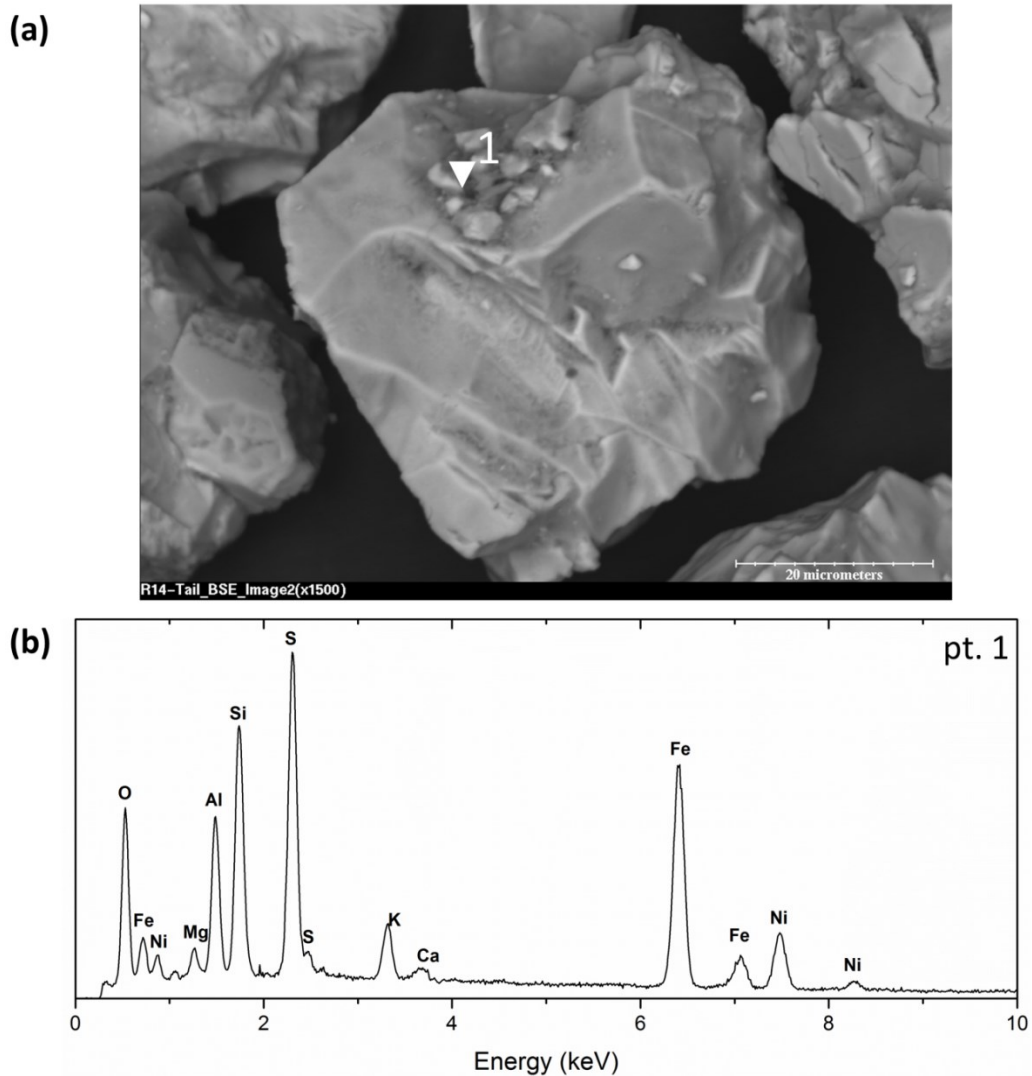
Figure 4-9 The (a) SEM image and (b) EDX spectrum of the pentlandite partially coated with magnesium silicate slime particles at pH 2.5.

The effect of olivine (Ol) fines on pentlandite recovery at pH 10.1 and pH 2.5 are shown in Figure 4-10a and 4-10b, respectively. At pH 10.1, the pentlandite recovery at Ol concentration of 1.3% and 4% were 89.9% (Figure 4-10a, ■) and 82.1% (Figure 4-10a, ▲), respectively. Increasing the amount of olivine fines threefold slightly reduced pentlandite recovery at pH 10.1. At pH 2.5, the pentlandite recovery at Ol concentration of 1.3% and 4% were 95.0% (Figure 4-10b, ■) and 95.6% (Figure 4-10b, ▲), respectively. Increasing the amount of olivine fines did not impact pentlandite recovery at pH 2.5. The final pentlandite recovery was higher at pH 2.5 than at pH 10.1. The initial flotation rate, however, was higher at pH 10.1 than at pH 2.5.

Figure 4-10 Recovery of pentlandite as a function of time and olivine fines concentration (a) at pH 10.1, and (b) at pH 2.5 in 1 mM KCl and 5 x 10^{-4} M PAX solution (■ – Ol = 1.3%), ▲ – Ol = 4%).

Figure 4-11 shows the X-Ray map of the non-floating component from the pentlandite-serpentine flotation at pH 10.1. The map indicates a substantial presence of Mg and Si containing particles, which can be ascribed to the presence

of olivine. Based on the X-Ray map, the amount of pentlandite was not significant as compared to the amount of olivine. This may indicate a higher selectivity of pentlandite to olivine in the flotation at pH 10.1.
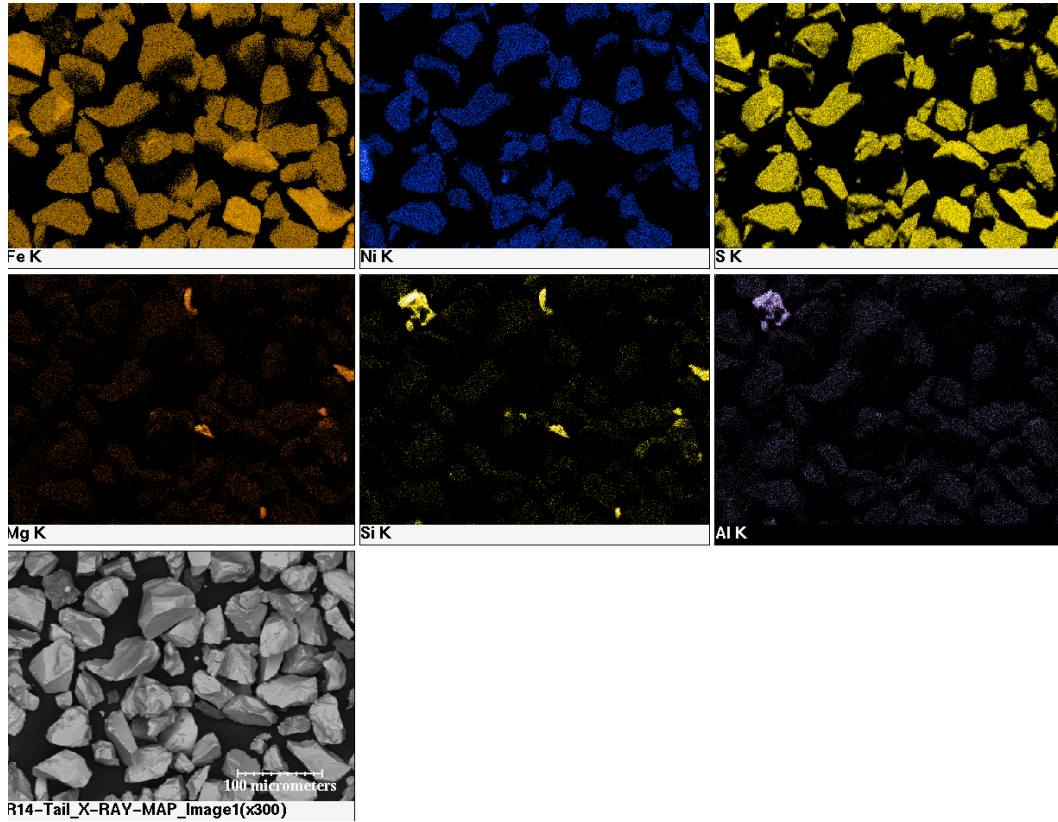

Figure 4-11 X-Ray mapping of the non-floating component from the pentlandite-olivine flotation at pH 10.1 in 1 mM KCl solution.

Figure 4-12 shows the X-Ray map of the non-floating component from the pentlandite-olivine flotation at pH 2.5. The map indicates the presence of both olivine (as indicated by Mg, Al, Si elements) and pentlandite (as indicated by Fe, Ni, S elements) on the tailing.

Figure 4-12 X-Ray mapping of the non-floating component from the pentlandite-olivine flotation at pH 2.5 in 1 mM KCl solution.

The effect of magnesite (Mg) fines on pentlandite recovery at pH 10.1 and pH 2.5 are shown in Figure 4-13a and 4-13b, respectively. At pH 10.1, the pentlandite recovery at Mg concentration of 1.3% and 4% were 87.8% (Figure 4-13a, ■) and 75.7% (Figure 4-13a, ▲), respectively. Increasing the amount of olivine fines threefold reduced pentlandite recovery by 12.1% at pH 10.1, indicating that the amount of magnesite fines affected pentlandite recovery. At pH 2.5, the pentlandite recovery at Mg concentration of 1.3% and 4% were 95.1% (Figure 4-13b, ■) and 93.6% (Figure 4-13b, ▲), respectively. It should be noted that at acidic pH, magnesite has higher solubility (Gence, 2006). The final pentlandite

recovery was significantly higher at pH 2.5 than at pH 10.1. The pentlandite recovery at pH 2.5 was close to the recovery after the pentlandite flotation without the presence of magnesite. Nevertheless, the initial flotation rate was higher at pH 10.1 than at pH 2.5.
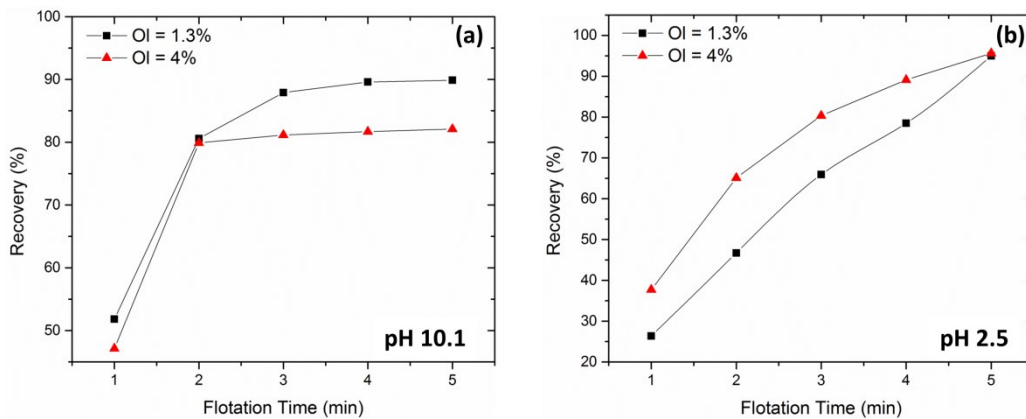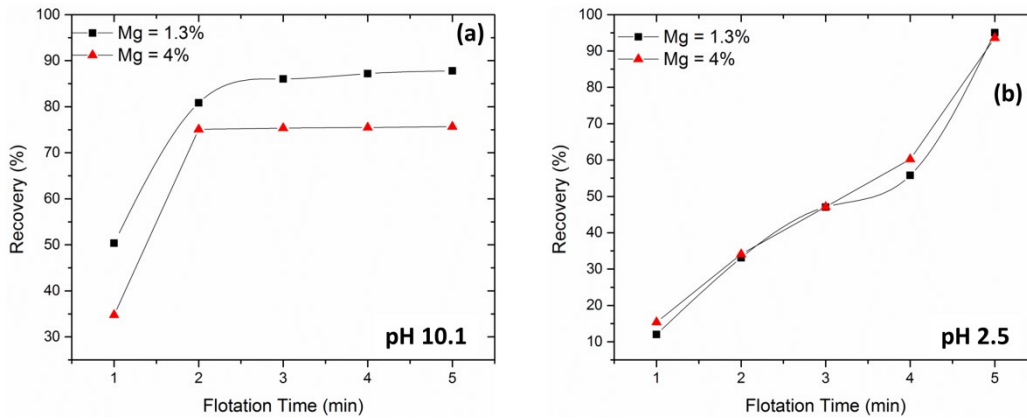

Figure 4-13 Recovery of pentlandite as a function of time and magnesite fines concentration (a) at pH 10.1, and (b) at pH 2.5 in 1 mM KCl and 5 x 10^{-4} M PAX solution (■ – Mg = 1.3%), ▲ – Mg = 4%).

Figure 4-14 shows the X-Ray map of the non-floating component from the pentlandite-magnesite flotation at pH 10.1. The map indicates the substantial presence of magnesite (as indicated by Mg elements). The shape and location of magnesite fines can be determined by comparing the map of Mg element with the SEM image of the map. Judging by the amount of magnesite in the map, the flotation selectivity is quite significant in the pentlandite-magnesite system.
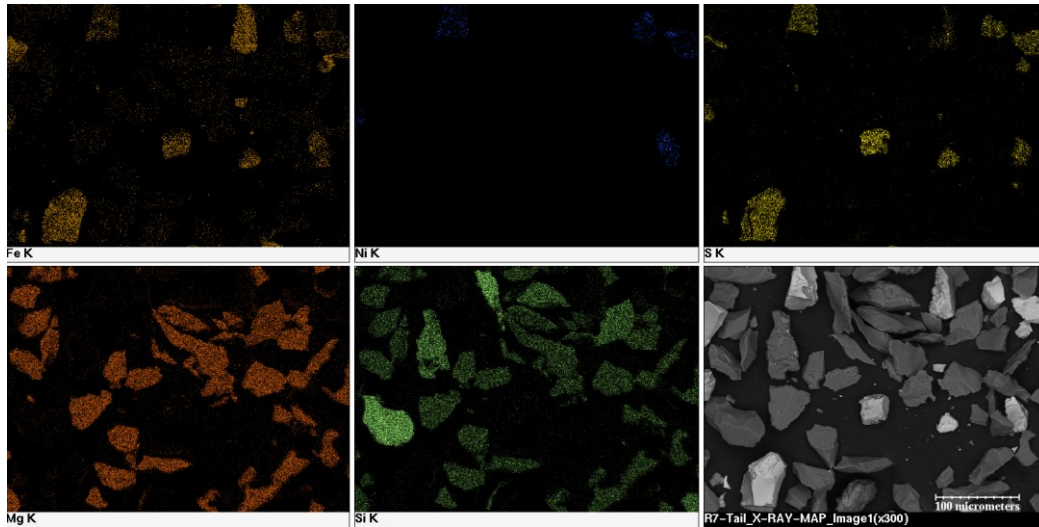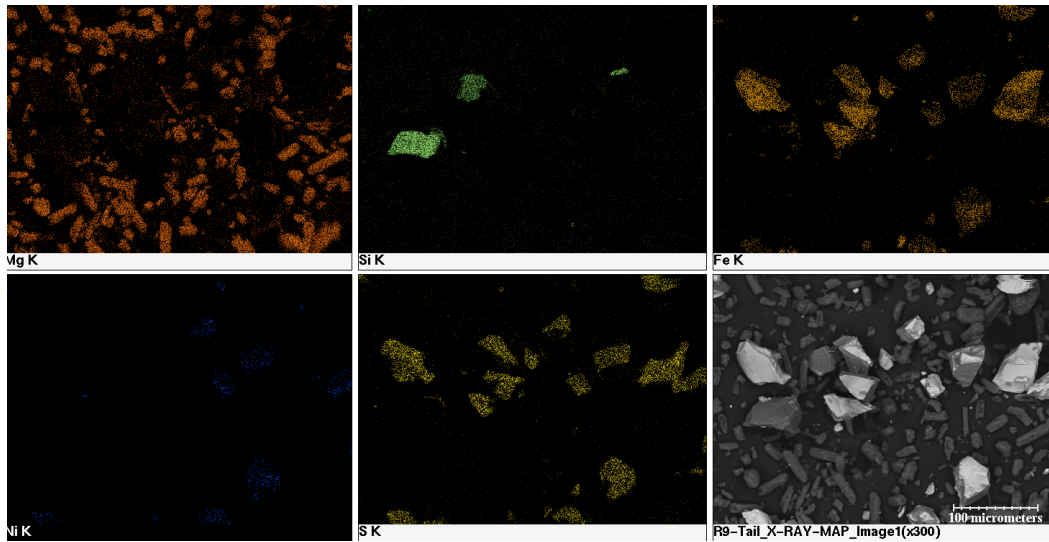
Figure 4-14 X-Ray mapping of the non-floating component from the pentlandite-magnesite flotation at pH 10.1 in 1 mM KCl solution.

Figure 4-15 shows the X-Ray map of the non-floating component from the pentlandite-magnesite flotation at pH 2.5. As opposed to the non-floating component from pH 10.1, the map indicates no presence of magnesite fines. The magnesite fines which were observed in Figure 4-14 were not found in Figure 4-15. The Mg element observed from the map was possibly originated from the magnesium silicate impurities on pentlandite sample. At pH 2.5, magnesite fines were fully dissolved due to the higher solubility at this acidic condition.
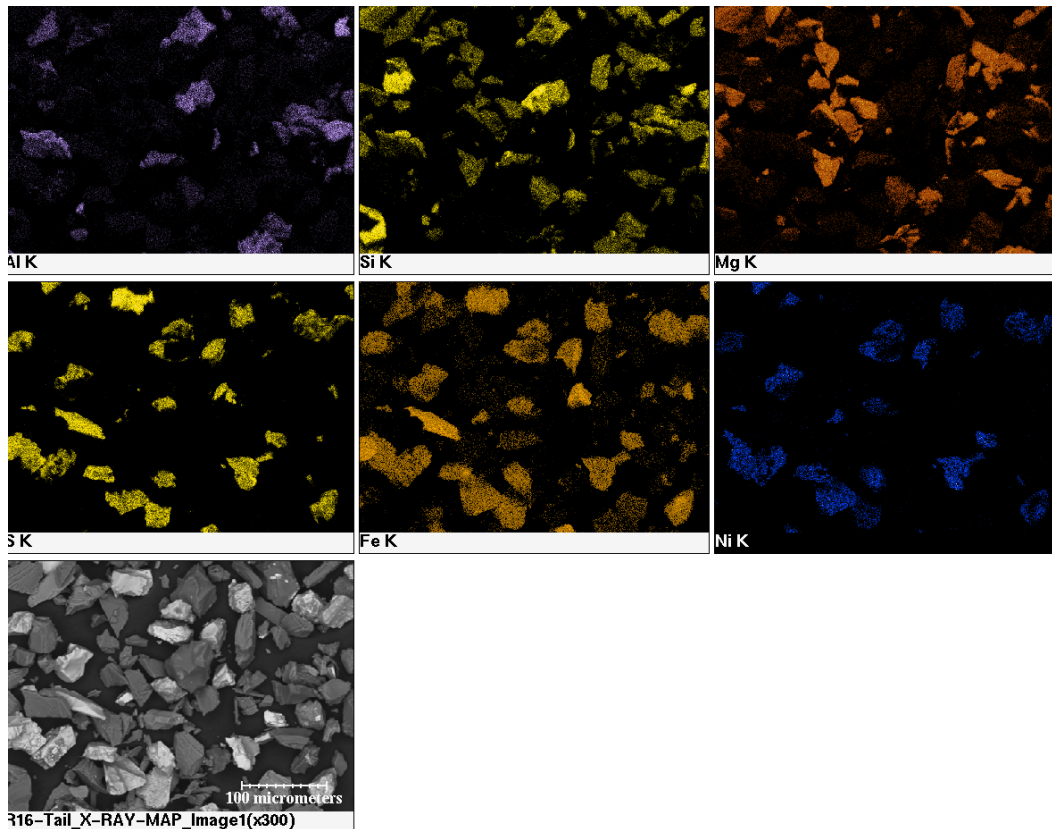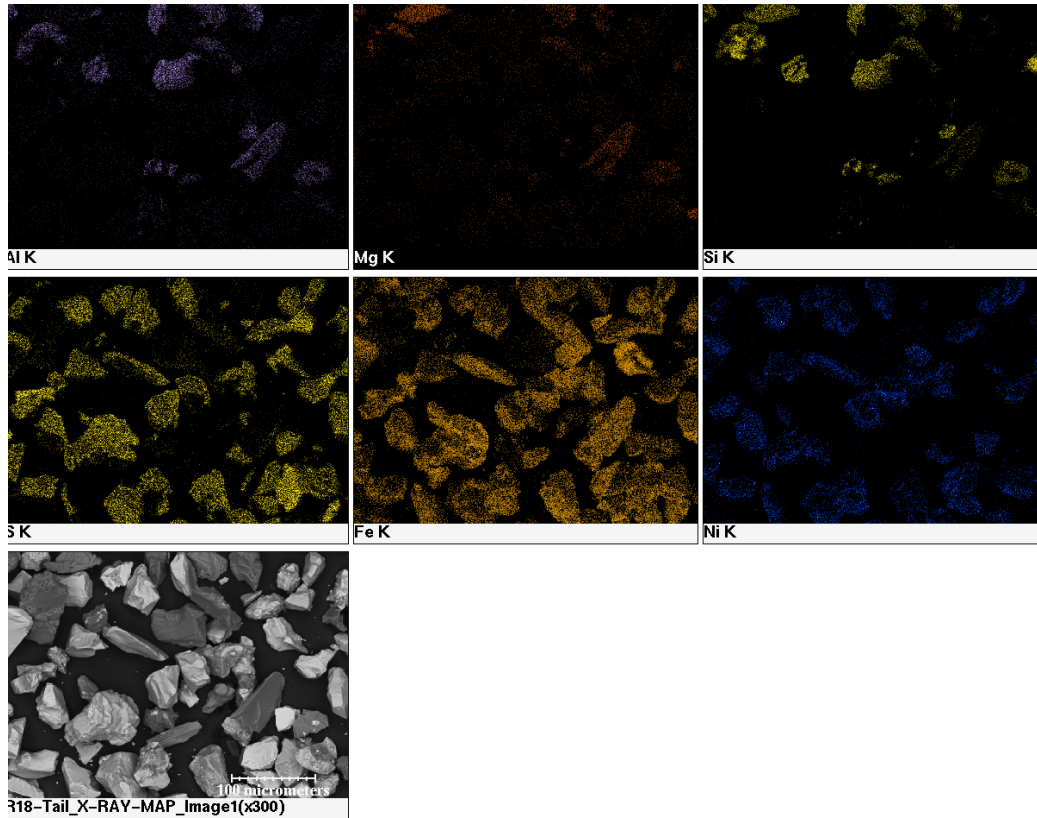
Figure 4-15 X-Ray mapping of the non-floating component from the pentlandite-magnesite flotation at pH 2.5 in 1 mM KCl solution.

Table 4-3 summarizes the pentlandite recovery after flotation in the presence of different gangue minerals and at different pH. The presence of serpentine depressed pentlandite recovery more significantly than when olivine or magnesite was present. Increasing the serpentine to pentlandite weight ratio also further depressed pentlandite recovery. This is mainly due to the slime coating of serpentine on pentlandite surface which has been observed previously (Edwards et al., 1980).

The higher pentlandite recovery in the presence of olivine and magnesite fines at pH 10.1 can be explained by considering the zeta potential of pentlandite, olivine,

and magnesite. Previous investigation by Kusuma et al. (2013) showed that pentlandite, olivine, and magnesite were all negatively charged at pH 10.1. Therefore, the formation of slime coating can be obstructed, leading to a greater surface area on pentlandite surface and allowing air bubble attachment during flotation. Similar observation is found in the flotation of pentlandite in the presence of quartz at alkaline pH, where the negatively charged quartz does not affect the recovery of the negatively charged pentlandite (Feng et al., 2012).

At pH 2.5, serpentine slime coating may be present on pentlandite surface, in which an attractive electrostatic interaction occurred between a positively charged pentlandite and a negatively charged silica face of serpentine. At pH 2.5, both pentlandite and olivine were positively charged (Kusuma et al., 2013). Due to the similar charges of olivine and pentlandite, olivine slime coating on pentlandite surface can be avoided, leading to higher pentlandite recovery. The presence of magnesite did not affect pentlandite flotation at pH 2.5, since magnesite was dissolved in an acidic solution. Therefore there was no depression on pentlandite recovery.

It should be noted that xanthate collector decomposes at acidic pH (Iwasaki and Cooke, 1958). Therefore the mechanism of pentlandite attachment to the air bubble is due to the more hydrophobic characteristic of pentlandite at pH 2.5 (Alvarez-Silva, 2011). Even though the recovery is higher at pH 2.5, previous study has shown that flotation at natural or acidic pH resulted in a concentrate that had lower Ni grade than that obtained through flotation at pH 10.1 (Dai et al., 2009). This is mainly due to the lower flotation selectivity between pentlandite

and magnesium silicate gangue minerals at lower pH, which results in a higher MgO grade of the concentrate. Flotation at low pH also activates the flotation iron sulphides, which further reduces the Ni grade of the concentrate (Dai et al., 2009). Therefore, flotation at low pH results in poorer concentrate upgradability than the concentrate obtained from flotation at pH 10.1.

Table 4-3 Pentlandite recovery in the presence of different gangue minerals and at different pH.

Fines	Fines concentration (%)	Pentlandite recovery (%)	
		pH 2.5	pH 10.1
Serpentine	1.3	78.8	73.8
	4	54.3	46.6
Olivine	1.3	95.0	89.9
	4	95.6	82.1
Magnesite	1.3	95.1	87.8
	4	93.6	75.7
No fines	N/A	97.3	89.7

4.4 Conclusions

Our study has shown that different gangue minerals (i.e. serpentine, olive, magnesite) demonstrated different impact on the flotation of pentlandite. In addition, contact angle and induction time measurements were employed to study the hydrophobicity of gangue and valuable minerals. Among the gangue minerals,

olivine is more hydrophobic than serpentine and magnesite, as observed from the contact angle and induction time measurements; while pentlandite, as the valuable mineral, is also more hydrophobic than the gangue minerals. The presence of serpentine in the flotation significantly depresses pentlandite recovery at pH 10.1; whereas the presence of olivine and magnesite does not significantly depress pentlandite recovery at pH 10.1. At pH 2.5, pentlandite recovery was higher than the recovery at pH 10.1. However, the presence of serpentine also depresses pentlandite recovery at pH 2.5. In general, the depression effect increases with the increasing fine minerals concentration. It is believed that strong electrostatic attraction between serpentine and pentlandite may lead to a slime coating on pentlandite surface and cause the detrimental depression of pentlandite recovery at pH 10.1. Therefore, at the operational pH of 10.1, it can be predicted that the presence of olivine or magnesium does not significantly affect the recovery of pentlandite.

4.5 References

Alvarez-Silva, M. (2011) *Surface chemistry study on the pentlandite-serpentine system, PhD Dissertation*, McGill University.

Alvarez-Silva, M., Mirnezami, M., Uribe-Salas, A., Finch, J.A. (2010a) 'Point of zero charge, isoelectric point and aggregation of phyllosilicate minerals', *Canadian Metallurgical Quarterly*, vol. 49, no. 4, pp. 405–410.

Alvarez-Silva, M., Uribe-Salas, A., Mirnezami, M., Finch, J.A. (2010b) 'The
point of zero charge of phyllosilicate minerals using the Mular-Roberts
titration technique', *Minerals Engineering*, vol. 23, pp. 383–389.

Beattie, D.A., Huynh, L., Kaggwa, G.B., Ralston, J. (2006) 'Influence of adsorbed
polysaccharides and polyacrylamides on talc flotation', *International
Journal of Mineral Processing*, vol. 78, no. 4, pp. 238–249.

Bremmel, K.E., Fornasiero, D., Ralston, J. (2005) 'Pentlandite-lizardite
interactions and implications for their separation by flotation', *Colloids
and Surfaces A: Physicochemical and Engineering Aspects*, vol. 252, pp.
207–212.

Chau, T.T., Bruckard, W.J., Koh, P.T.L., Nguyen, A.V. (2009) 'A review of
factors that affect contact angle and implications for flotation practice',
Advances in Colloid and Interface Science, vol. 150, pp. 106–115.

Dai, Z., Bos, J.A., Quinn, P., Lee, A., Xu, M. (2009) 'Flowsheet development for
Thompson ultramafic low-grade nickel ores', *Proceedings of the 48th
annual conference of metallurgists of CIM*, Met Soc, Sudbury, Ontario,
Canada, pp. 217–228.

Edwards, C.R., Kipkie, W.B., Agar, G.E. (1980) 'The effect of slime coatings of
the serpentine minerals, chrysotile and lizardite, on pentlandite flotation',
International Journal of Mineral Processing, vol. 7, pp. 33–42.

Feng, B., Feng, Q., Lu, Y. (2012) 'A novel method to limit the detrimental effect of serpentine on the flotation of pentlandite', *International Journal of Mineral Processing*, vol. 114-117, pp. 11–13.

Feng, B., Lu, Y., Feng, Q., Ding, P., Luo, N. (2013) 'Mechanisms of surface charge development of serpentine mineral', *Transactions of Nonferrous Metals Society of China*, vol. 23, pp. 1123–1128.

Gence, N. (2006) 'Wetting behavior of magnesite and dolomite surfaces', *Applied Surface Science*, vol. 252, no. 10, pp. 3744–3750.

Gualtieri, A.F., Gemmi, M., Dapiaggi, M. (2003) 'Phase transformations and reaction kinetics during the temperature-induced oxidation of natural olivine', *American Mineralogist*, vol. 88, pp. 1560–1574.

Gualtieri, A.F., Giacobbe, C., Viti, C. (2012) 'The dehydroxylation of serpentine group minerals', *American Mineralogist*, vol. 97, pp. 666–680.

Gupta, V., Miller, J.D. (2010) 'Surface force measurements at the basal planes of ordered kaolinite particles', *Journal of Colloid and Interface Science*, vol. 344, pp. 362–371.

Huang, Z., Li, W., Pan, Z., Liu, Y., Fang, M. (2013) 'High-temperature transformation of asbestos tailings by carbothermal reduction', *Clays and Clay Minerals*, vol. 61, no. 1, pp. 75-82.

Iwasaki, I., Cooke, S.R. (1958) 'The decomposition of xanthate in acid solution', *Journal of the American Chemical Society*, vol. 80, no. 2, pp. 285-288.

Kusuma, A., Zeng, H., Liu, Q. (2013) 'Understanding mineral interaction mechanisms by zeta potential and surface force measurements', *Proceedings of the Procemin 2013 10th International Mineral Processing Conference*, Gecamin, Santiago, Chile, pp. 407–415.

Leonelli, C., Veronesi, P., Boccaccini, D.N., Rivasi, M.R., Barbieri, L., Andreola, F., Lancellotti, I., Rabitti, D., Pellacani, G.C. (2006) 'Microwave thermal inertisation of asbestos containing waste and its recycling in traditional ceramics', *Journal of Hazardous Materials B*, vol. 135, pp. 149-155.

Lu, Y., Long, T., Feng, Q., Ou, L., Zhang, G. (2009) 'Flotation and its mechanisms of fine serpentine', *The Chinese Journal of Nonferrous Metals*, vol. 19, no. 8, pp. 1493-1497.

Merve Genc, A., Kilickaplan, I., Laskowski, J.S. (2012) 'Effect of pulp rheology on flotation of nickel sulphide ore with fibrous gangue particles', *Canadian Metallurgical Quarterly*, vol. 51, no. 4, pp. 368–375.

Miller, J.D., Nalaskowski, J., Abdul, B., Du, H. (2007) 'Surface characteristics of kaolinite and other selected two layer silicate minerals', *The Canadian Journal of Chemical Engineering*, vol. 85, pp. 617-624.

Minowa, T., Yoshikawa, M., Honshima, M. (1989) 'Improvement of the corrosion resistance on Nd-Fe-B magnet with nickel plating', *IEEE Transactions on Magnetics*, vol. 25, no. 5, pp. 3776–3778.

Mookherjee, M., Stixrude, L. (2009) 'Structure and elasticity of serpentine at high-pressure', *Earth and Planetary Science Letters*, vol. 279, pp. 11–19.

Parks, G.A. (1965) 'The isoelectric points of solid oxides, solid hydroxides, and aqueous hydroxo complex systems', *Chemical Reviews*, vol. 65, no. 2, pp. 177-198.

Parks, G.A. (1967) 'Aqueous surface chemistry of oxides and complex minerals', In *Equilibrium Concepts in Natural Water Systems*, pp. 121-160, American Chemical Society.

Pietrobon, M.C., Grano, S.R., Sobieraj, S., Ralston, J. (1997) 'Recovery mechanisms for pentlandite and MgO-bearing gangue minerals in nickel ores from Western Australia', *Minerals Engineering*, vol. 10, no. 8, pp. 775–786.

Rahilly, G., Price, N. (2003) 'Current products and practice Nickel allergy and orthodontics', *Journal of Orthodontics*, vol. 30, pp. 171–174.

Rao, S.R. (1971) *Xanthates and related compounds*, M. Dekker, New York.

Senior, G.D., Thomas, S.A. (2005) 'Development and implementation of a new flowsheet for the flotation of a low grade nickel ore', *International Journal of Mineral Processing*, vol. 78, pp. 49–61.

Su, L., Xu, Z., Masliyah, J. (2006) 'Role of oily bubbles in enhancing bitumen flotation', *Minerals Engineering*, vol. 19, pp. 641–650.

Wellham, E.J., Elber, L., Yan, D.S. (1992) 'The role of carboxy methyl cellulose in the flotation of a nickel sulphide transition ore', *Minerals Engineering*, vol. 5, no. 3-5, pp. 381–395.

Xu, M., Dai, Z., Dong, J., Ford, F., Lee, A. (2010) 'Fibrous minerals in ultramafic nickel sulphide ores', *Proceedings of the 49th annual conference of metallurgists*, Met Soc, Vancouver, British Columbia, Canada, pp. 223–235.

Ye, Y., Miller, J.D. (1988) 'Bubble/particle contact time in the analysis of coal flotation', *Coal Preparation*, vol. 5, no. 3-4, pp. 147–166.

Zhang, Q., Wu, M., Zhao, W. (2005) 'Electroless nickel plating on hollow glass microspheres', *Surface and Coatings Technology*, vol. 192, pp. 213–219.

Zussman, J. (1978) 'The crystal structures of amphibole and serpentine minerals', *Proceedings of the workshop on asbestos, definitions and measurement method*, The Bureau, Maryland, pp. 35–48.

Chapter 5 Conclusions and Contributions

5.1 Major conclusions

This thesis work is divided in two parts. The first part examined the interaction between different gangue minerals (i.e. serpentine, olivine, magnesite) and pentlandite. This was investigated through zeta potential distribution and direct interaction force measurements (by using an AFM). The second part examined the effect of different gangue minerals towards pentlandite recovery in series of flotation tests. The major findings and conclusions of this thesis are summarized as follows:

1) Pentlandite and serpentine have strong attractive interaction, as observed in the zeta potential distribution measurements at pH 10.1 in 10 mM KCl solution. This explains the slime coating of serpentine on pentlandite surface.

2) A repulsive interaction is present in pentlandite-olivine and pentlandite-magnesite systems, as indicated from the zeta potential distribution measurements at pH 10.1 in 10 mM KCl solution.

3) From the AFM force measurement at pH 10.1 in 1 mM KCl solution, a repulsive interaction is present between the silicon nitride tip and serpentine surface. This is possibly due to the measurement being taken on the silica face of serpentine.

4) The AFM force measurement at pH 10.1 in 1 mM KCl solution between the silicon nitride tip and olivine surface shows a repulsive interaction. This

supports the repulsive interaction observed in the zeta potential distribution measurement of the pentlandite and olivine system.

5) The AFM force measurement at pH 10.1 in 1 mM KCl solution between the silicon nitride tip and magnesite surface shows a slight attractive interaction, which is mainly due to the van der Waals attraction.

6) Among the gangue minerals, olivine is more hydrophobic than serpentine and magnesite, as observed from the contact angle and induction time measurements at pH 10.1 in 10 mM KCl solution.

7) The presence of serpentine in the flotation significantly depresses pentlandite recovery at pH 10.1; whereas the presence of olivine and magnesite does not significantly reduce pentlandite recovery at the same pH. In general, increasing the concentration of the fine gangue minerals reduces pentlandite recovery during flotation.

5.2 Contributions to the original knowledge

In this study, the interaction between gangue minerals (i.e. serpentine, olivine, magnesite) and pentlandite, and their impact towards pentlandite recovery during flotation were investigated. Previous studies mainly focus on the interaction between serpentine and pentlandite, and its relation to pentlandite flotation. However, this study is the first of its kind to include and to investigate the effect of olivine and magnesite as gangue minerals. Furthermore, measurements using zeta potential distribution and AFM were the first to be employed to study the interaction between pentlandite and different gangue minerals. The results from

this study have provided better understanding of the impact of different gangue minerals in the pentlandite flotation.

Chapter 6 Future Work

6.1 Future work

1) In this study, a silicon nitride AFM tip was used to represent the negative charge of pentlandite mineral at pH 10.1. The direct interaction force measurement between pentlandite and gangue minerals (i.e. serpentine, olivine, magnesite) can be performed by attaching a pentlandite particle on a tipless AFM cantilever using a glue. However, several factors such as particle geometry and the inability to image a surface must be taken into account. These factors may make it difficult to fit the force curve with the DLVO theory.

2) A specially made AFM tip may be created, by coating or growing the AFM tip such that the tip has similar chemical compositions as pentlandite. This may result in an AFM tip with a known geometry. Hence, the force profile obtained by using this specially made tip may be fitted using DLVO theory.

3) The streaming potential measurement on serpentine surface should be investigated to compare with the measurement by electrophoresis technique. This is due to the heterogeneous structure of serpentine (layer by layer structure).

4) The surface isolation of serpentine mineral worths investigating. By isolating the silica tetrahedral and brucite octahedral layers, direct interaction force measurements can be performed on these surfaces.

5) In addition to the presence of gangue minerals, the flotation tests may also be performed in the presence of carboxymethyl cellulose (CMC), which a typical dispersant used in industry. It would be interesting to see the effect of the presence of both gangue minerals and CMC.

6) Perform the flotation tests by using larger equipment, such as Denver Cell. By using larger equipment, it would be interesting to investigate a wider range of the amount of gangue minerals on pentlandite recovery.

Bibliography

Alvarez-Silva, M. (2011) *Surface chemistry study on the pentlandite-serpentine system, PhD Dissertation*, McGill University.

Alvarez-Silva, M., Mirnezami, M., Uribe-Salas, A., Finch, J.A. (2010) 'Point of zero charge, isoelectric point and aggregation of phyllosilicate minerals', *Canadian Metallurgical Quarterly*, vol. 49, no. 4, pp. 405–410.

Alvarez-Silva, M., Uribe-Salas, A., Mirnezami, M., Finch, J.A. (2010b) 'The point of zero charge of phyllosilicate minerals using the Mular-Roberts titration technique', *Minerals Engineering*, vol. 23, pp. 383–389.

Baas-Becking, L.G., Galliher, E.W. (1931) 'Wall structure and mineralization in coralline algae', *The Journal of Physical Chemistry*, vol. 35, no. 2, pp. 467-479.

Beattie, D.A., Huynh, L., Kaggwa, G.B., Ralston, J. (2006) 'Influence of adsorbed polysaccharides and polyacrylamides on talc flotation', *International Journal of Mineral Processing*, vol. 78, no. 4, pp. 238–249.

Berg, J.C. (2010) *An introduction to interfaces and colloids: The bridge to nanoscience*, World Scientific, Singapore.

Bergström, L. (1997) 'Hamaker constants of inorganic materials', *Advances in Colloid and Interface Science*, vol. 70, pp. 125-169.

Binnig, G., Rohrer, H. (1983) 'Scanning Tunneling Microscopy', *Surface Science*, vol. 126, pp. 236–244.

Binnig, G., Quate, C.F., Gerber, C. (1986) 'Atomic Force Microscope', *Physical Review Letters*, vol. 56, no. 9, pp. 930–933.

Bobicki, E.R., Liu, Q., Xu, Z. (2014) 'Microwave heating of ultramafic nickel ores and mineralogical effects', *Minerals Engineering*, vol. 58, pp. 22-25.

Bozkurt, V., Xu, Z., Finch, J.A. (1999) 'Effect of depressants on xanthate adsorption on pentlandite and pyrrhotite: Single vs mixed minerals', *Canadian Metallurgical Quarterly*, vol. 38, no. 2, pp. 105-112.

Bremmel, K.E., Fornasiero, D., Ralston, J. (2005) 'Pentlandite-lizardite interactions and implications for their separation by flotation', *Colloids and Surfaces A: Physicochemical and Engineering Aspects*, vol. 252, pp. 207–212.

Brindley, G. W., Hayami, R. (1964) 'Kinetics and mechanisms of dehydration and recrystallization of serpentine: I', *Clays and Clay Minerals*, vol. 12, pp. 35-47.

Butt, H.J., Cappella, B., Kappl, M. (2005) 'Force measurements with the atomic force microscope: Technique, interpretation and applications', *Surface Science Reports*, vol. 59, pp. 1–152.

Cattaneo, A., Gualtieri, A. F., Artioli, G. (2003) 'Kinetic study of the dehydroxylation of chrysotile asbestos with temperature by in situ XRPD', *Physics and Chemistry of Minerals*, vol. 30, no. 3, pp. 177-183.

Chau, T.T., Bruckard, W.J., Koh, P.T.L., Nguyen, A.V. (2009) 'A review of factors that affect contact angle and implications for flotation practice', *Advances in Colloid and Interface Science*, vol. 150, pp. 106–115.

Dai, Z., Bos, J.A., Quinn, P., Lee, A., Xu, M. (2009) 'Flowsheet development for Thompson ultramafic low-grade nickel ores', *Proceedings of the 48th annual conference of metallurgists of CIM*, Met Soc, Sudbury, Ontario, Canada, pp. 217–228.

Dalvi, A.D., Bacon, W.G., Osborne, R.C. (2004) 'The past and the future of nickel laterites', In *PDAC 2004 International Convention, Trade Show & Investors Exchange*, Toronto: The Prospectors and Developers Association of Canada, pp. 1–27.

Drelich, J., Long, J., Yeung, A. (2007) 'Determining surface potential of the bitumen-water interface at nanoscale resolution using atomic force microscopy', *The Canadian Journal of Chemical Engineering*, vol. 85, no. 5, pp. 625–634.

Ducker, W.A., Senden, T.J., Pashley, R.M. (1991) 'Direct measurement of colloidal forces using an atomic force microscope', *Nature*, vol. 353, no. 6341, pp. 239–241.

Ducker, W.A., Senden, T.J., Pashley, R.M. (1992) 'Measurement of forces in liquids using a force microscope', *Langmuir*, vol. 8, no. 7, pp. 1831–1836.

Edwards, C.R., Kipkie, W.B., Agar, G.E. (1980) 'The effect of slime coatings of the serpentine minerals, chrysotile and lizardite, on pentlandite flotation', *International Journal of Mineral Processing*, vol. 7, pp. 33–42.

Fan, X., Rowson, N.A. (2000) 'Fundamental investigation of microwave pretreatment on the flotation of massive ilmenite ores', *Developments in Chemical Engineering and Mineral Processing*, vol. 8, pp. 167-182.

Feng, B., Feng, Q., Lu, Y. (2012a) 'A novel method to limit the detrimental effect of serpentine on the flotation of pentlandite', *International Journal of Mineral Processing*, vol. 114-117, pp. 11–13.

Feng, B., Lu, Y., Feng, Q., Zhang, M., Gu, Y. (2012b) 'Talc-serpentine interactions and implications for talc depression', *Minerals Engineering*, vol. 32, pp. 68–73.

Feng, B., Lu, Y., Feng, Q., Ding, P., Luo, N. (2013) 'Mechanisms of surface charge development of serpentine mineral', *Transactions of Nonferrous Metals Society of China*, vol. 23, no. 4, pp. 1123–1128.

Fuerstenau, D.W., Pradip. (2005) 'Zeta potentials in the flotation of oxide and silicate minerals', *Advances in Colloid and Interface Science*, vol. 114-115, pp. 9–26.

Game, P.M. (1941) 'Optical properties of olivines from Ubekendt Island, West Greenland', *Mineralogical Magazine*, vol. 26, no. 172, pp. 11–15.

Gence, N. (2006) 'Wetting behavior of magnesite and dolomite surfaces', *Applied Surface Science*, vol. 252, no. 10, pp. 3744–3750.

Gualtieri, A.F., Gemmi, M., Dapiaggi, M. (2003) 'Phase transformations and reaction kinetics during the temperature-induced oxidation of natural olivine', *American Mineralogist*, vol. 88, pp. 1560–1574.

Gualtieri, A.F., Giacobbe, C., Viti, C. (2012) 'The dehydroxylation of serpentine group minerals', *American Mineralogist*, vol. 97, pp. 666–680.

Gupta, V., Miller, J.D. (2010) 'Surface force measurements at the basal planes of ordered kaolinite particles', *Journal of Colloid and Interface Science*, vol. 344, pp. 362–371.

Haque, K.E. (1999) 'Microwave energy for mineral treatment processes – a brief review', *International Journal of Mineral Processing*, vol. 57, pp. 1–24.

Hayes, R.A., Price, D.M., Ralston, J., Smith, R.W. (1987) 'Collectorless flotation of sulphide minerals', *Mineral Processing and Extractive Metallurgy Review*, vol. 2, no. 3, pp. 203-234.

Hayes, R.A., Ralston, J. (1988) 'The collectorless flotation and separation of sulphide minerals by E_h control', *International Journal of Mineral Processing*, vol. 23, pp. 55-84.

Holuszko, M.E., Franzidis, J.P., Manlapig, E.V., Hampton, M.A., Donose, B.C., Nguyen, A.V. (2008) 'The effect of surface treatment and slime coatings on ZnS hydrophobicity', *Minerals Engineering*, vol. 21, pp. 958–966.

Huang, Z., Li, W., Pan, Z., Liu, Y., Fang, M. (2013) 'High-temperature transformation of asbestos tailings by carbothermal reduction', *Clays and Clay Minerals*, vol. 61, no. 1, pp. 75-82.

Israelachvili, J. (2011) *Intermolecular and surface forces*, 3rd ed., Academic Press, London.

Iwasaki, I., Cooke, S.R. (1958) 'The decomposition of xanthate in acid solution', *Journal of the American Chemical Society*, vol. 80, no. 2, pp. 285-288.

Kelebek, S., Wells, P.F., Fekete, S.O. (1996) 'Differential flotation of chalcopyrite, pentlandite and pyrrhotite in Ni-Cu sulphide ores', *Canadian Metallurgical Quarterly*, vol. 35, no. 4, pp. 329-336.

Kusuma, A., Zeng, H., Liu, Q. (2013) 'Understanding mineral interaction mechanisms by zeta potential and surface force measurements', *Proceedings of the Procemin 2013 10th International Mineral Processing Conference*, Gecamin, Santiago, Chile, pp. 407–415.

Leonelli, C., Veronesi, P., Boccaccini, D.N., Rivasi, M.R., Barbieri, L., Andreola, F., Lancellotti, I., Rabitti, D., Pellacani, G.C. (2006) 'Microwave thermal inertisation of asbestos containing waste and its recycling in traditional ceramics', *Journal of Hazardous Materials B*, vol. 135, pp. 149-155.

Lin, X.Y., Creuzet, F., Arribart, H. (1993) 'Atomic force microscopy for local characterization of surface acid-base properties', *Journal of Physical Chemistry*, vol. 97, pp. 7272–7276.

Liu, J., Zhou, Z., Xu, Z., Masliyah, J. (2002) 'Bitumen-clay interactions in aqueous media studied by zeta potential distribution measurement', *Journal of Colloid and Interface Science*, vol. 252, pp. 409–418.

Liu, J., Xu, Z., Masliyah, J. (2003) 'Studies on bitumen-silica interaction in aqueous solutions by atomic force microscopy', *Langmuir*, vol. 19, pp. 3911–3920.

Liu, J., Xu, Z., Masliyah, J. (2004a) 'Interaction between bitumen and fines in oil sands extraction system: implication to bitumen recovery', *The Canadian Journal of Chemical Engineering*, vol. 82, no. 4, pp. 655–666.

Liu, J., Xu, Z., Masliyah, J. (2004b) 'Role of fine clays in bitumen extraction from oil sands', *AIChE Journal*, vol. 50, no. 8, pp. 1917–1927.

Liu, J., Xu, Z., Masliyah, J. (2005) 'Interaction forces in bitumen extraction from oil sands', *Journal of Colloid and Interface Science*, vol. 287, no. 2, pp. 507–520.

Lu, Y., Long, T., Feng, Q., Ou, L., Zhang, G. (2009) 'Flotation and its mechanisms of fine serpentine', *The Chinese Journal of Nonferrous Metals*, vol. 19, no. 8, pp. 1493-1497.

Lu, Y., Zhang, M., Feng, Q., Long, T., Ou, L., Zhang, G. (2011) 'Effect of sodium hexametaphospate on separation of serpentine from pyrite', *Transactions of Nonferrous Metals Society of China*, vol. 21, pp. 208-213.

Masliyah, J., Czarnecki, J., Xu, Z. (2011) *Handbook on theory and practice of bitumen recovery from Athabasca oil sands*, Kingsley, Canada.

Merve Genc, A., Kilickaplan, I., Laskowski, J.S. (2012) 'Effect of pulp rheology on flotation of nickel sulphide ore with fibrous gangue particles', *Canadian Metallurgical Quarterly*, vol. 51, no. 4, pp. 368–375.

Miller, J.D., Nalaskowski, J., Abdul, B., Du, H. (2007) 'Surface characteristics of kaolinite and other selected two layer silicate minerals', *The Canadian Journal of Chemical Engineering*, vol. 85, pp. 617-624.

Minowa, T., Yoshikawa, M., Honshima, M. (1989) 'Improvement of the corrosion resistance on Nd-Fe-B magnet with nickel plating', *IEEE Transactions on Magnetics*, vol. 25, no. 5, pp. 3776–3778.

Mookherjee, M., Stixrude, L. (2009) 'Structure and elasticity of serpentine at high-pressure', *Earth and Planetary Science Letters*, vol. 279, pp. 11–19.

Mooney, T., Knacke, R.F. (1985) 'Optical constants of chlorite and serpentine between 2.5 and 50 μm', *Icarus*, vol. 64, pp. 493–502.

Moskalyk, R.R., Alfantazi, A.M. (2002) 'Nickel laterite processing and electrowinning practice', *Minerals Engineering*, vol. 15, pp. 593–605.

Mudd, G.M. (2010) 'Global trends and environmental issues in nickel mining: Sulfides versus laterites', *Ore Geology Reviews*, vol. 38, pp. 9–26.

Müller, P. (1994) 'Glossary of terms used in physical organic chemistry (IUPAC Recommendations 1994)', Pure and Applied Chemistry, vol. 66, no. 5, pp. 1077–1184.

Myers, D. (1999) *Surfaces, interfaces, and colloids: Principles and applications*, 2nd ed., John Wiley & Sons, New York.

nickel (Ni). (2014) In *Encyclopaedia Britannica*, Retrieved in 6 January 2014, <http://www.britannica.com/EBchecked/topic/414238/nickel>.

Niederhauser, M., Wisdom, T. (2013) 'The tailings evolution: Advancements, benefits, and challenges', *Proceedings of the Procemin 2013 10th International Mineral Processing Conference*, Gecamin, Santiago, Chile, pp. 569.

Nishikawa, K., Takahashi, K., Karjalainen, A., Wen, C., Furuya, S., Hoshuyama, T., Todoroki, M., Kiyomoto, Y., Wilson, D., Higashi, T., Ohtaki, M., Pan, G.W., Wagner, G. (2008) 'Recent mortality from pleural mesothelioma, historical patterns of asbestos use, and adoption of bans: A global assessment', *Environmental Health Perspectives*, vol. 116, pp. 1675–1680.

Osasere, O.F. (2000) 'Relation of contact angle data to Hallimond tube flotation of coal with coagulants and flocculants', *Fuel*, vol. 79, pp. 193–199.

Parks, G.A. (1965) 'The isoelectric points of solid oxides, solid hydroxides, and aqueous hydroxo complex systems', *Chemical Reviews*, vol. 65, no. 2, pp. 177-198.

Parks, G.A. (1967) 'Aqueous surface chemistry of oxides and complex minerals', In *Equilibrium Concepts in Natural Water Systems*, pp. 121-160, American Chemical Society.

Pietrobon, M.C., Grano, S.R., Sobieraj, S., Ralston, J. (1997) 'Recovery mechanisms for pentlandite and MgO-bearing gangue minerals in nickel ores from Western Australia', *Minerals Engineering*, vol. 10, no. 8, pp. 775–786.

Pokrovsky, O.S., Schott, J. (2004) 'Experimental study of brucite dissolution and precipitation in aqueous solutions: Surface speciation and chemical affinity control', *Geochimica et Cosmochimica Acta*, vol. 68, no. 1, pp. 31–45.

Pollock, T.M., Tin, S. (2006) 'Nickel-based superalloys for advanced turbine engines: Chemistry, microstructure, and properties', *Journal of Propulsion and Power*, vol. 22, no. 2, pp. 361–374.

Rahilly, G., Price, N. (2003) 'Current products and practice Nickel allergy and orthodontics', *Journal of Orthodontics*, vol. 30, pp. 171–174.

Rao, S.R. (1971) *Xanthates and related compounds*, M. Dekker, New York.

Rao, S.R., Leja, J. (2004) *Surface chemistry of froth flotation*, Kluwer Academic Publishers, New York, USA.

Rosenholtz, J.L., Smith, D.T. (1936) *The dielectric constant of mineral powders*, Rensselaer Polytechnic Institute.

Sedore, L. (2003) *MgO rejection from Birchtree ore at Inco's Manitoba division, Master of Engineering Thesis*, McGill University.

Senior, G.D., Thomas, S.A. (2005) 'Development and implementation of a new flowsheet for the flotation of a low grade nickel ore', *International Journal of Mineral Processing*, vol. 78, pp. 49–61.

Su, L., Xu, Z., Masliyah, J. (2006) 'Role of oily bubbles in enhancing bitumen flotation', *Minerals Engineering*, vol. 19, pp. 641–650.

Uddin, S., Rao, S.R., Mirnezami, M., Finch, J.A. (2012) 'Processing an ultramafic ore using fiber disintegration by acid attack', *International Journal of Mineral Processing*, vol. 102-103, pp. 38–44.

Viti, C. (2010) 'Serpentine minerals discrimination by thermal analysis', *American Mineralogist*, vol. 95, no. 4, pp. 631-638.

Wei, Z., Fusheng, Y., Yuangang, L., Jianlin, Q., Anning, Z. (2011) 'Influence of microwave treatment under a hydrogen or methane atmosphere on the flotability of the macerals in Shenfu coals', *Mining Science and Technology (China)*, vol. 21, pp. 761–766.

Wellham, E.J., Elber, L., Yan, D.S. (1992) 'The role of carboxy methyl cellulose in the flotation of a nickel sulphide transition ore', *Minerals Engineering*, vol. 5, no. 3-5, pp. 381–395.

Xu, Z., Liu, J., Choung, J.W., Zhou, Z. (2003) 'Electrokinetic study of clay interactions with coal in flotation', *International Journal of Mineral Processing*, vol. 68, pp. 183-196.

Xu, M., Dai, Z., Dong, J., Ford, F., Lee, A. (2010) 'Fibrous minerals in ultramafic nickel sulphide ores', *Proceedings of the 49th annual conference of*

metallurgists, Met Soc, Vancouver, British Columbia, Canada, pp. 223–235.

Yan, L., Englert, A.H., Masliyah, J.H., Xu, Z. (2011) 'Determination of anisotropic surface characteristics of different phyllosilicates by direct force measurements', *Langmuir*, vol. 27, pp. 12996–13007.

Yan, L., Masliyah, J.H., Xu, Z. (2013) 'Understanding suspension rheology of anisotropically-charged platy minerals from direct interaction force measurement using AFM', *Current Opinion in Colloid & Interface Science*, vol. 18, pp. 149-156.

Ye, Y., Miller, J.D. (1988) 'Bubble/particle contact time in the analysis of coal flotation', *Coal Preparation*, vol. 5, no. 3-4, pp. 147–166.

Yin, X., Drelich, J. (2008) 'Surface charge microscopy: novel technique for mapping charge-mosaic surfaces in electrolyte solutions', *Langmuir*, vol. 24, pp. 8013–8020.

Yoon, R.H., Yordan, J.L. (1991) 'Induction time measurements for the quartz-amine flotation system', *Journal of Colloid and Interface Science*, vol. 141, no. 2, pp. 374-383.

Yuan, Y., Lee, T.R. (2013) 'Contact angle and wetting properties', In Bracco, G. & Holst, B. (eds.), *Surface Science Techniques*, pp. 3–34, Springer-Verlag Berlin Heidelberg.

Zhang, Q., Wu, M., Zhao, W. (2005) 'Electroless nickel plating on hollow glass microspheres', *Surface and Coatings Technology*, vol. 192, pp. 213–219.

Zhao, H., Bhattacharjee, S., Chow, R., Wallace, D., Masliyah, J., Xu, Z. (2008) 'Probing surface charge potentials of clay basal planes and edges by direct force measurements', *Langmuir*, vol. 24, pp. 12899–12910.

Zussman, J. (1978) 'The crystal structures of amphibole and serpentine minerals', *Proceedings of the workshop on asbestos, definitions and measurement method*, The Bureau, Maryland, pp. 35–48.